



Proline biosynthesis is a vent for TGF β -induced mitochondrial redox stress

Simon Schwörer¹ , Mirela Berisa², Sara Violante², Weige Qin², Jiajun Zhu¹, Ronald C Hendrickson³, Justin R Cross² & Craig B Thompson^{1,*} 

Abstract

The production and secretion of matrix proteins upon stimulation of fibroblasts by transforming growth factor-beta (TGF β) play a critical role in wound healing. How TGF β supports the bioenergetic cost of matrix protein synthesis is not fully understood. Here, we show that TGF β promotes protein translation at least in part by increasing the mitochondrial oxidation of glucose and glutamine carbons to support the bioenergetic demand of translation. Surprisingly, we found that in addition to stimulating the entry of glucose and glutamine carbon into the TCA cycle, TGF β induced the biosynthesis of proline from glutamine in a Smad4-dependent fashion. Metabolic manipulations that increased mitochondrial redox generation promoted proline biosynthesis, while reducing mitochondrial redox potential and/or ATP synthesis impaired proline biosynthesis. Thus, proline biosynthesis acts as a redox vent, preventing the TGF β -induced increase in mitochondrial glucose and glutamine catabolism from generating damaging reactive oxygen species (ROS) when TCA cycle activity exceeds the ability of oxidative phosphorylation to convert mitochondrial redox potential into ATP. In turn, the enhanced synthesis of proline supports TGF β -induced production of matrix proteins.

Keywords collagen; fibrosis; metabolism; proline; TGF β

Subject Categories Cell Adhesion, Polarity & Cytoskeleton; Metabolism; Signal Transduction

DOI 10.15252/emj.2019103334 | Received 28 August 2019 | Revised 1 February 2020 | Accepted 4 February 2020 | Published online 5 March 2020

The EMBO Journal (2020) 39: e103334

Introduction

Mammalian cells depend on extracellular signals for growth, proliferation, and survival. In the absence of adequate extrinsic signals, cells cannot maintain viability due to an inability to take up nutrients (Rathmell *et al*, 2000). Growth factor-directed nutrient uptake is critical to sustain cellular bioenergetics as well as the biosynthesis of macromolecules required for a cell to grow and proliferate. Glucose

and glutamine are the major carbon sources for ATP production and biosynthesis, and glutamine provides the nitrogen required for biosynthesis (Altman *et al*, 2016; Hosios *et al*, 2016). Binding of receptor tyrosine kinases (RTKs) by extracellular growth factors promotes both the uptake and utilization of glucose and glutamine. For example, stimulation of RTKs can activate PI3K/AKT/mTOR signaling to increase surface localization of transporters for glucose and amino acids, and to promote utilization of these nutrients for glycolysis, anabolic cell growth, and survival (Lien *et al*, 2016).

Growth factor-induced uptake of nutrients often exceeds a cell's need for maintenance of bioenergetics and biosynthesis (Bauer *et al*, 2004). Oxidation of carbon substrates in the tricarboxylic acid (TCA) cycle creates electrons that are transferred to nicotinamide adenine dinucleotide (NAD⁺) and flavin adenine dinucleotide (FAD), yielding NADH and FADH₂. NADH and FADH₂ then donate electrons to the electron transport chain (ETC) at complexes I and II, creating an electron flow to complexes III and IV, and finally, to molecular oxygen, generating water. However, increased carbon oxidation in the TCA cycle in response to growth factor stimulation can yield NADH levels that exceed the capacity of the ETC to transfer electrons to molecular oxygen or the ability of complex V to dissipate the ETC-produced proton gradient through ATP production (Murphy, 2009; Wellen & Thompson, 2010). This increases the chance of mitochondrial hyperpolarization, resulting in production of reactive oxygen species (ROS) which can damage the cell (Murphy, 2009; Schieber & Chandel, 2014). Certain cell types including liver, muscle, or adipose cells can store excess glucose carbon in the form of glycogen and fat. However, most cells in the human body are unable to store extra glucose. Therefore, to protect themselves from excessive mitochondrial ROS generation, these cells limit oxidation of glucose-derived carbon (Thompson, 2011). Proliferating cells adapt by secreting excess glycolytic carbon in the form of lactate, often mediated by ROS-induced HIF-1 α signaling (Lum *et al*, 2007; Vander Heiden *et al*, 2009). There are also efflux pathways for glycolytic pyruvate that enters the TCA cycle. Citrate secreted from the mitochondria supports lipid biosynthesis required for proliferation (Bauer *et al*, 2005); aspartate, generated from the TCA cycle intermediate oxaloacetate, is exported from the mitochondria to support nucleotide biosynthesis and protein translation (Birsoy

¹ Cancer Biology and Genetics Program, Sloan Kettering Institute, Memorial Sloan Kettering Cancer Center, New York, NY, USA

² Donald B. and Catherine C. Marron Cancer Metabolism Center, Sloan Kettering Institute, Memorial Sloan Kettering Cancer Center, New York, NY, USA

³ Microchemistry and Proteomics Core, Sloan Kettering Institute, Memorial Sloan Kettering Cancer Center, New York, NY, USA

*Corresponding author. Tel: +1 212 639 6561; Fax: +1 212 717 3299; E-mail: thompsonc@mskcc.org

et al., 2015; Sullivan *et al.*, 2015). Thus, cell growth is directly coupled to the utilization of these metabolic “vents”, conferring proliferating cells with a mechanism to prevent ROS accumulation under growth factor stimulation. Another major nutrient reported to be under growth factor control is glutamine. Glutamine uptake in most transformed cells has been reported to be driven by myc-dependent increase in glutamine uptake and mitochondrial deamination to produce glutamate and alpha-ketoglutarate which support transamination reactions and TCA cycle anaplerosis, respectively (Wise *et al.*, 2008; Gao *et al.*, 2009). However, it is less clear how cells adapt to the accumulation of glutamine-derived metabolites and prevent them from further increasing mitochondrial ROS as they enter the TCA cycle.

Unlike most extracellular growth factors, transforming growth factor-beta-1 (TGF β -1, hereafter TGF β) does not bind to an RTK but activates a heterodimeric receptor with serine/threonine kinase activity, resulting in phosphorylation of Smad2 or Smad3 proteins which then bind to Smad4. Smad2/3-Smad4 complexes bind to DNA and are responsible for the vast majority of TGF β -induced transcriptional output (Siegel & Massagué, 2003). The cellular responses to TGF β are often context-dependent; for example, TGF β is known for its growth-constraining and immunosuppressive effects, but it is also a potent inducer of epithelial–mesenchymal transition and fibrosis (Massagué, 2012). Recent evidence indicates that activation of TGF β signaling supports these processes at least in part by reprogramming cellular metabolism. For instance, TGF β -mediated activation and differentiation of fibroblasts into extracellular matrix (ECM)-producing myofibroblasts are accompanied by an increase in glucose uptake, glycolytic metabolism, and activation of the serine/glycine biosynthetic pathway (Andrianifahanana *et al.*, 2016; Nigdelioglu *et al.*, 2016; Selvarajah *et al.*, 2019). In addition, glutaminolysis is required for TGF β -induced collagen production (Bernard *et al.*, 2018; Hamanaka *et al.*, 2019).

Here, we report that, unlike growth factors such as PDGF or IGF that primarily stimulate glucose metabolism, TGF β stimulates both glucose and glutamine metabolism. Metabolic tracing experiments demonstrate that in TGF β -stimulated cells, glutamine that enters the mitochondria is preferentially used to support proline biosynthesis rather than TCA cycle anaplerosis. However, we observed that a rise in cellular proline levels in response to TGF β was preceded by increased mitochondrial oxidative activity. We show that the TGF β -induced increase in proline occurs when TCA cycle oxidation exceeds the electron assimilation capacity of the electron transport chain. We propose that Smad4-dependent induction of proline biosynthesis protects cells from the damaging effects of TGF β -induced increase in TCA cycle activity by diverting excess mitochondrial redox potential into the production of proline and supporting enhanced translation of collagens.

Results

TGF β selectively promotes translation in serum-stimulated fibroblasts

To study the primary response of fibroblasts to TGF β stimulation in the presence of other growth factors, a condition that occurs during wound healing (Barrientos *et al.*, 2008), we treated NIH-3T3

fibroblasts for up to 72 h with TGF β in the presence of 10% serum. During this period, TGF β did not stimulate cell proliferation (Fig 1A). Nevertheless, TGF β potently elevated the translation rate as measured by the incorporation of O-propargyl-puromycin, a tRNA-mimetic compound, into nascent polypeptides (Figs 1B and EV1A). TGF β treatment increased the expression of matrix proteins as reported by others (Fig 1C; Ignatz & Massagué, 1986), and we measured a higher deposition of collagens and fibronectin in cell-derived ECM (Fig 1D–F). Similar observations were made in human lung fibroblasts (Fig EV1B and C). To sustain an increased translation rate, cells require high levels of ATP, both for charging of tRNAs with their cognate amino acid and for the regeneration of GTP which is consumed during elongation of the polypeptide chain. Consistent with a higher demand for ATP to meet the bioenergetic demand of increased translation, TGF β treatment resulted in elevated consumption of glucose (Fig 1G) and increased the rate of ATP synthesis (Fig 1H). Both ATP production from glycolysis and oxidative phosphorylation were increased (Fig 1H).

As reported by others (Nigdelioglu *et al.*, 2016; Selvarajah *et al.*, 2019), TGF β -stimulated cells displayed a higher glycolytic activity (Fig EV1D–F). We found that the increase in glucose uptake is an early event in response to TGF β stimulation and plateaus after 24 h (Fig EV1G). Lactate secretion following TGF β treatment showed similar kinetics (Fig EV1H) and is in proportion to the glucose taken up by TGF β -stimulated cells (Fig EV1I). Thus, lactate production per molecule glucose remained similar before and after TGF β stimulation (Fig EV1J) and the amount of glucose utilized and not secreted as lactate also increases. Thus, TGF β -stimulated cells retain increased levels of glucose carbon to support biosynthesis and mitochondrial ATP production.

Using a kinetic analysis, we find that TGF β -induced translation and mitochondrial ATP production significantly correlated with each other (Figs 1I and EV1K and L), suggesting that an increase in oxidative phosphorylation is coupled to protein synthesis. In addition to glucose, TGF β stimulated consumption of glutamine (Figs 1J and EV1M), which can act as anaplerotic substrate to support the TCA cycle (Deberardinis *et al.*, 2007). To confirm that TGF β stimulated oxidative phosphorylation, we measured the oxygen consumption rate on a Seahorse Bioanalyzer. This analysis demonstrated that TGF β potently stimulated mitochondrial respiration and increased substrate availability to the electron transport chain (maximal respiration) (Fig 1K). An increased rate of protein synthesis and mitochondrial oxygen consumption in response to TGF β treatment was also observed under serum-deprived conditions (Fig EV1N and O).

Despite the increase in oxidative metabolism, cellular ROS production was not elevated in cells grown in TGF β -containing medium, as measured by the ratio of reduced/oxidized glutathione and the general ROS indicator DCFDA (Fig 1L and M). Taken together, these results indicate that TGF β promotes nutrient uptake and mitochondrial oxidation primarily to support cellular bioenergetics and translation of ECM proteins, without increasing either cell proliferation or oxidative stress.

TGF β promotes proline synthesis from glutamine for collagen production

In addition to ATP, translation requires a continuous supply of amino acids for tRNA charging. Since TGF β stimulated the synthesis

of matrix proteins, but not growth, we hypothesized that TGFβ treatment induces the accumulation of intracellular amino acids that are particularly enriched in matrix proteins relative to other

proteins. The amino acid composition of collagens, the most abundant proteins in the human body and in the ECM, is significantly different from that of other proteins (Fig 2A); compared to other

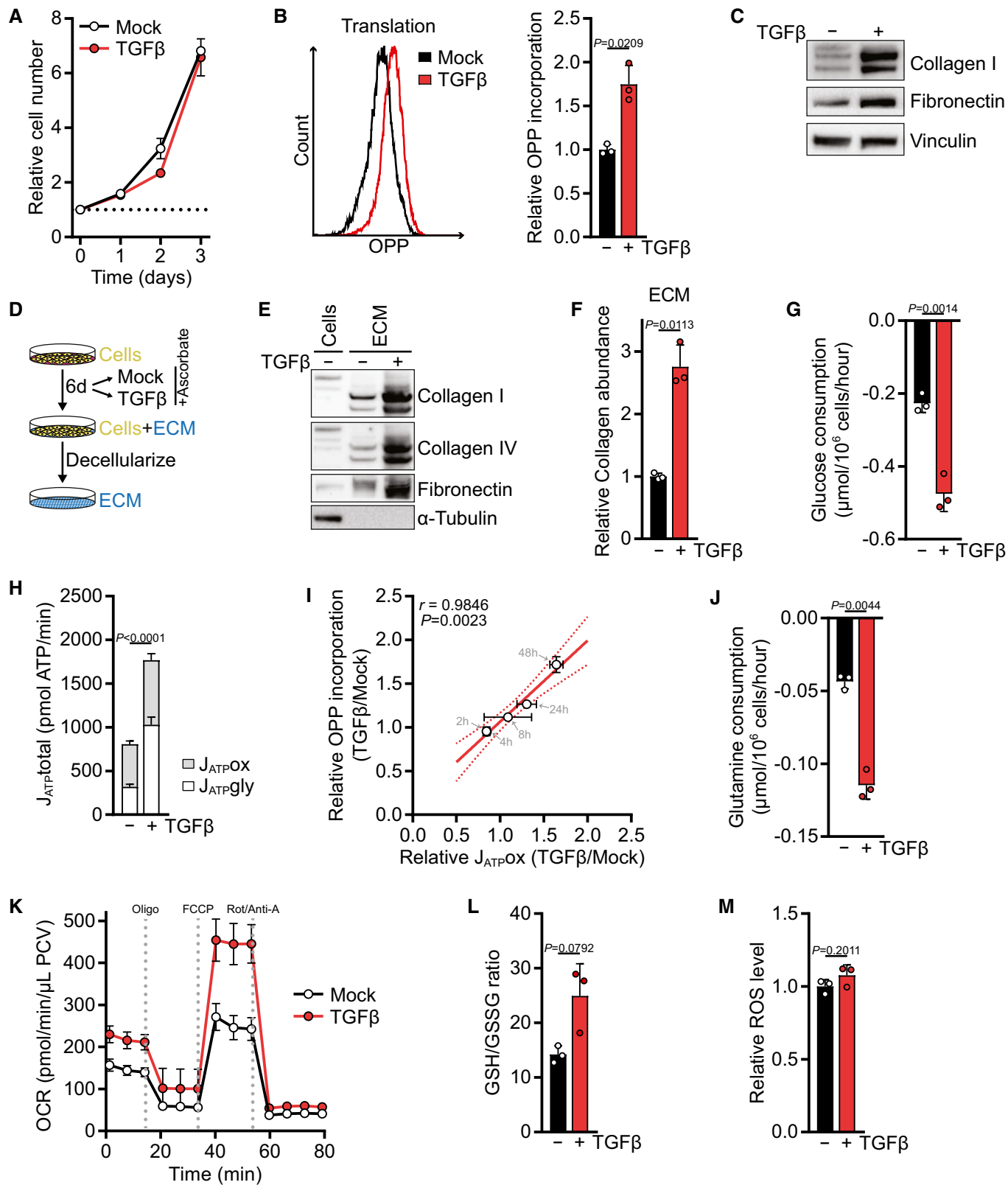


Figure 1.

Figure 1. TGF β selectively promotes translation in serum-stimulated fibroblasts.

- A Growth curve of NIH-3T3 cells treated with TGF β (2 ng/ml for all experiments) or vehicle alone (mock) for the indicated time. The cell number at the indicated days relative to the number at the start of the treatment (d0) is shown. The dotted line represents the cell number at d0.
- B NIH-3T3 cells were treated with TGF β or mock for 48 h and incubated with O-propargyl-puromycin (OPP) for the last 60 min. The translation rate was determined by flow cytometry for OPP incorporation into proteins. A representative plot is shown on the left, and the quantification is shown on the right. Values are relative to mock-treated cells.
- C Western blot of NIH-3T3 cells treated with TGF β or mock for 48 h.
- D Schematic of extracellular matrix (ECM) production *in vitro*.
- E Western blot of ECM from NIH-3T3 cells grown in the presence or absence of TGF β and of cell lysates from NIH-3T3 cells grown on a parallel plate. Note the absence of tubulin and the electromobility shift of collagens in ECM extracts.
- F ECM was produced from NIH-3T3 cells according to (D), and collagen abundance was measured by picosirius red staining, normalized to the packed cell volume before ECM extraction, and expressed relative to mock-treated cells.
- G NIH-3T3 cells were treated with TGF β or mock for 48 h. The medium was replaced in the last 12 h of the treatment (with the same treatments as before), and glucose consumption from the fresh media was measured using the YSI bioanalyzer.
- H ATP production rate from glycolysis (J_{ATPgly}) and mitochondrial oxidative phosphorylation (J_{ATPOx}) from NIH-3T3 cells treated with TGF β or mock for 48 h, calculated using Seahorse data shown in (K) and Fig EV1F.
- I Pearson's correlation of mitochondrial ATP production rate (J_{ATPOx}) and OPP incorporation of NIH-3T3 cells treated with TGF β or mock for 2, 4, 8, 24 and 48 h, relative to mock-treated cells. Also see Fig EV1K and L. Note that the data points of the 2- and 4-h measurements overlap.
- J Glutamine consumption measured as in (G).
- K NIH-3T3 cells were treated with TGF β or mock for 48 h, and the oxygen consumption rate (OCR) before and after treatment with mitochondrial inhibitors was measured using the Seahorse bioanalyzer. Oligo, oligomycin; Rot/Anti-A, rotenone/antimycin; PCV, packed cell volume.
- L NIH-3T3 cells were treated with TGF β or mock for 48 h, and reduced (GSH) and oxidized (GSSG) glutathione were measured by LC-MS/MS. Shown is the GSH/GSSG ratio.
- M NIH-3T3 cells were treated with TGF β for 48 h or mock and incubated with CM-H₂DCFDA for the last 30 min. ROS were measured by flow cytometry for CM-H₂DCFDA. Values are relative to mock-treated cells.
- Data information: *P*-values were calculated by two-sided unpaired *t*-test with Welch's correction (B, F–H, J, L, M) or by Pearson's correlation analysis (I). Bars in (B, F–H, J, L, M) represent the mean \pm SD; data in (A, I, K) represent the mean \pm SD; and line in (I) represents linear regression with the SD shown as dotted lines. *n* = 3 (A, B, F, G, J, L, M); *n* = 8 (H, K); *n* = 5 (I). A representative experiment is shown (B, C, E).

proteins, collagens are particularly enriched in glycine (Fig 2A). To verify this in living cells, we performed acid hydrolysis of proteins isolated from NIH-3T3 cells and their secreted ECM and confirmed a significant increase in the representation of glycine in cell-derived ECM compared to total cellular protein (Fig 2B).

It has been reported that in addition to stimulating ATP production, glucose catabolism promotes glycine synthesis in the glycolytic pathway via serine from the glycolytic intermediate 3-phosphoglycerate (Fig EV2A). To test whether TGF β diverts glycolytic carbons into glycine biosynthesis, we traced the fate of glucose uniformly labeled with [¹³C] at all six carbons ([U-¹³C] Glc). This analysis demonstrated that TGF β stimulated the synthesis of both serine and glycine from glucose (Fig EV2B and C). In addition, TGF β also increased labeling of citrate and downstream TCA cycle metabolites from glucose (Fig EV2D–G). These data are in line with a higher availability of glucose for both biosynthesis and mitochondrial oxidation upon TGF β stimulation. We also assessed the contribution of glutamine to glycine biosynthesis. While glutamine carbon did not contribute to serine and glycine (Fig EV2H), both serine and glycine were substantially labeled by the glutamine alpha-nitrogen (Fig EV2I). TGF β treatment further increased alpha-nitrogen labeling of serine and glycine (Fig EV2I), consistent with TGF β -induced expression of PSAT1 (Hamanaka *et al*, 2019) which catalyzes the transamination reaction in the serine biosynthetic pathway.

The second major amino acid enriched in collagens and the ECM is proline and its modified derivative hydroxyproline (Fig 2A and B). Since proline is a non-essential amino acid produced from glutamine (Fig EV3A), we tested whether TGF β promotes diversion of glutamine carbons into proline biosynthesis by tracing the fate of glutamine uniformly labeled with [¹³C] at all five carbons ([U-¹³C] Gln). Indeed, we found that TGF β treatment resulted in a substantial

increase in the fraction and abundance of proline labeled from glutamine (m+5) (Figs 2C and EV3B). In addition, TGF β -treated cells displayed an increase in the contribution of glutamine to glutamate (m+5) (Figs 2D and EV3B) and to all TCA cycle metabolites we measured via oxidative metabolism (m+4) (Figs 2E–H and EV3C). Based on the low percentage of labeling of later TCA cycle intermediates such as malate from glucose (Fig EV2F), these data suggest that TGF β -treated cells increase glutamine anaplerosis. In contrast, reductive synthesis of citrate (m+5), malate and aspartate (m+3) from glutamine was unchanged upon TGF β stimulation (Figs 2F–H and EV3D). Consistent with higher utilization of glutamine for proline biosynthesis and TCA cycle anaplerosis, glutaminase (GLS1) was upregulated in TGF β -treated cells (Fig EV3E).

Quantification of metabolic fluxes revealed that the flux of glutamine carbons into alpha-ketoglutarate was increased more than twofold in TGF β -treated cells and matched the elevated flux through glutaminase (Fig 2I). However, the flux of glutamine carbons into proline increased by sevenfold (Fig 2I). This was also reflected by a fourfold increase in free proline in cells upon treatment with TGF β , while the maximal increase in the abundance of glutamate and TCA cycle intermediates was 2.5-fold or less (Fig 2J). Proline levels were also increased when human lung fibroblasts were treated with TGF β (Fig EV3F). Since a significant amount of glutamate carbons were labeled from glucose (Fig EV2E), we also assessed whether glucose carbons contributed to proline. However, < 10% of proline carbon was labeled after 24 h of [U-¹³C] Glc tracing (Fig EV3G), indicating that glycolytic carbon does not substantially contribute to proline biosynthesis.

Glucose-derived glycine has been shown to be incorporated into collagen I (Nigdelioglu *et al*, 2016), but whether fibroblasts use glutamine-derived proline for the biosynthesis of collagen I is not

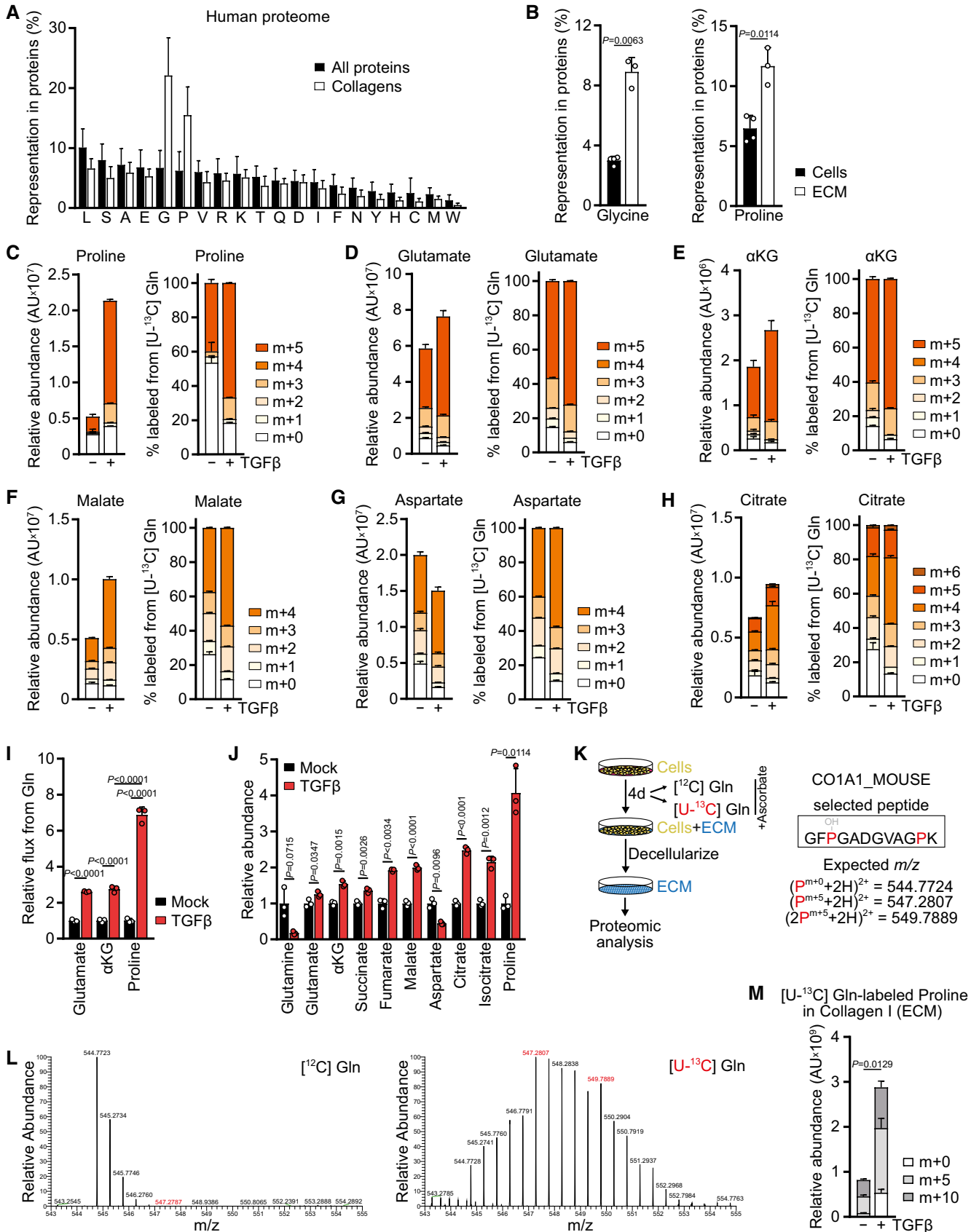


Figure 2.

Figure 2. TGFβ promotes proline synthesis from glutamine for collagen production.

- A Comparison of the amino acid representation in all human proteins and all collagens. The x-axis denotes individual amino acids shown by single-letter code.
- B Glycine and proline representation in protein acid hydrolysates of untreated NIH-3T3 cells and their secreted ECM, produced as in Fig 1D. Amino acids were measured by GC-MS.
- C–H Tracing of [^{13}C] L-glutamine ([^{13}C] Gln) into indicated metabolites. NIH-3T3 cells were treated with TGFβ (2 ng/ml for all experiments) or mock for 48 h, and the medium was replaced (including all treatments) with DMEM lacking L-glutamine and supplemented with [^{13}C] Gln for the last 8 h. Metabolic steady state was reached at this time point (see kinetic labeling curves in Fig EV3B). Metabolites were measured by LC-MS. The left graph shows the total pool size normalized to the packed cell volume; the right side shows the percent labeling. αKG, alpha-ketoglutarate; AU, arbitrary units.
- I Glutamine flux into glutamate, αKG, and proline in NIH-3T3 cells treated with TGFβ or mock for 48 h, relative to mock-treated cells.
- J Abundance of indicated metabolites in NIH-3T3 cells treated with TGFβ or mock for 48 h, relative to mock-treated cells. Metabolites were measured by GC-MS.
- K Schematic of [^{13}C] Gln tracing into proline in collagen I-α1 (CO1A1) in NIH-3T3 cell-derived ECM. Expected *m/z* of unlabeled (m+0) and fully labeled proline (m+5 for one proline, m+10 for two prolines) for the analytical peptide are shown.
- L Representative MS2 spectra of the CO1A1 peptide in ECM generated with unlabeled ([^{12}C] Gln, left) and fully labeled glutamine ([^{13}C] Gln, right). Peaks representing fully labeled (m+5, m+10) proline are highlighted in red. Peptides were measured by LC-MS.
- M Relative abundance of the analytical peptide containing unlabeled (m+0) or one/two fully labeled prolines (m+5/m+10) from the CO1A1 peptide in ECM derived from NIH-3T3 cells treated with TGFβ or mock in the presence of fully labeled L-glutamine ([^{13}C] Gln). Peptides were measured by LC-MS. The amount of ECM analyzed was normalized to the packed cell volume of cells grown on a parallel plate under identical conditions.

Data information: *P*-values were calculated by two-sided unpaired *t*-test with Welch's correction (B, J, M) or two-way ANOVA with Holm–Sidak multiple comparison test (I). Bars represent the mean + SD. *n* = 20,381 (all proteins), *n* = 44 (collagens) (A); *n* = 4 (cells), *n* = 3 (ECM) (B); *n* = 3 (C–J, M). A representative experiment is shown (L).

known. To test this, we cultured NIH-3T3 fibroblasts in the presence of unlabeled (^{12}C) or fully labeled (^{13}C) glutamine and extracted cell-derived ECM for proteomic analysis (Fig 2K). Glutamine carbons were readily incorporated as proline into collagen I secreted into the extracellular space (Figs 2L and EV3H), and the abundance of the collagen I peptide containing glutamine-derived proline increased with TGFβ treatment (Fig 2M). Taken together, these data demonstrate that TGFβ promotes the utilization of glucose and glutamine for both mitochondrial oxidation and biosynthesis of glycine and proline which are utilized for translation of collagens.

P5CS is required for proline biosynthesis and is upregulated in lung fibrosis patients

While the TGFβ-mediated stimulation of glycine biosynthesis has been reported (Nigdelioglu *et al*, 2016; Selvarajah *et al*, 2019), it is less well understood how TGFβ promotes proline biosynthesis. In particular, how TGFβ directs the preferential flux of glutamine carbon into proline biosynthesis over TCA cycle anaplerosis is unknown. Proline is made in mitochondria from glutamine-derived glutamate via two steps (Fig 3A): first, delta-1-pyrroline-5-carboxylate synthase (P5CS) catalyzes the ATP- and NADPH-dependent phosphorylation and reduction conversion of glutamate to gamma-glutamic semi-aldehyde (GSA), which is in equilibrium with delta-1-pyrroline-5-carboxylate (P5C). Pyrroline-5-carboxylate reductase family members 1 and 2 (PYCR1/2) further reduce P5C to proline in a reaction that preferentially uses NADH (de Ingeniis *et al*, 2012). We observed that, in addition to upregulating GLS1, TGFβ treatment elevated the expression of all enzymes in the mitochondrial proline biosynthetic pathway (Fig 3B). Similar observations were made in human lung fibroblasts (Fig EV4A). To test whether the induction of these enzymes is required for proline biosynthesis, we genetically disrupted all enzymes in the pathway by CRISPR/Cas9-mediated gene deletion. While deleting *Pycr1* or *Pycr2* individually did not affect cellular proline levels (Fig EV4B), proline was profoundly depleted in cells with deletion of *P5CS* encoded by aldehyde dehydrogenase 18 family member A1 (*Aldh18a1*, hereafter *P5CS*) (Fig 3C). Consistent with the high representation of

proline in collagens (Fig 2A), *P5CS* deletion diminished the expression of collagen I protein both in untreated and TGFβ-treated cells, which was restored by addition of proline to the culture medium (Fig 3D). Similar results were obtained when measuring collagen abundance in cell-derived ECM (Fig 3E).

We genetically engineered cells to overexpress *P5CS* to test whether the upregulation of *P5CS* by TGFβ contributes to increased proline and collagen biosynthesis. Indeed, ectopic expression of *P5CS* increased the abundance of proline in cells (Fig 3F) and elevated levels of collagen I in cells and the ECM (Fig 3G and H), although not to the same extent as did TGFβ stimulation. These data demonstrate that expression of *P5CS* is required and can be sufficient for proline and collagen biosynthesis in serum-stimulated cells growing in complete medium, and that collagen levels depend on mitochondrial proline biosynthesis.

Based on these findings, we hypothesized that *P5CS* expression could also be relevant for fibrotic diseases which are characterized by excessive deposition of collagen by chronically activated myofibroblasts. Focusing on idiopathic pulmonary fibrosis (IPF), the most severe and lethal fibrotic disease (Coultas *et al*, 1994), we analyzed *P5CS* expression in publicly available gene expression datasets from lungs of mice treated with bleomycin to induce pulmonary fibrosis or from lungs of IPF patients (Yang *et al*, 2013; Cecchini *et al*, 2018). We found that *P5CS* was significantly upregulated in the bleomycin mouse model of pulmonary fibrosis (Fig 3I) and in IPF patients compared to normal controls in two independent datasets (Fig 3J). Moreover, the forced vital capacity (FVC) as well as the diffusing capacity for carbon monoxide (DLCO), two independent parameters of lung function, inversely correlated with expression levels of *P5CS* in IPF patients (Figs 3K and EV4C). Taken together, these data show that *P5CS* expression is critical for proline and collagen biosynthesis and correlates with disease-relevant parameters.

Next, we investigated the regulation of proline biosynthesis by TGFβ using cells in which *Smad4* was deleted via CRISPR/Cas9 to abrogate *Smad4*-dependent transcription. While the increase in protein levels of proline biosynthetic enzymes in response to TGFβ was only partly regulated by *Smad4*, *Smad4* deletion abolished the induction of glutaminase upon TGFβ

treatment (Fig EV4D). The increase in labeling of proline and TCA cycle intermediates from glutamine in response to TGF β treatment was completely dependent on *Smad4* (Fig 3L),

suggesting that both the TGF β -mediated increase in TCA cycle anaplerosis and proline biosynthesis were regulated by *Smad4*-dependent glutaminase induction.

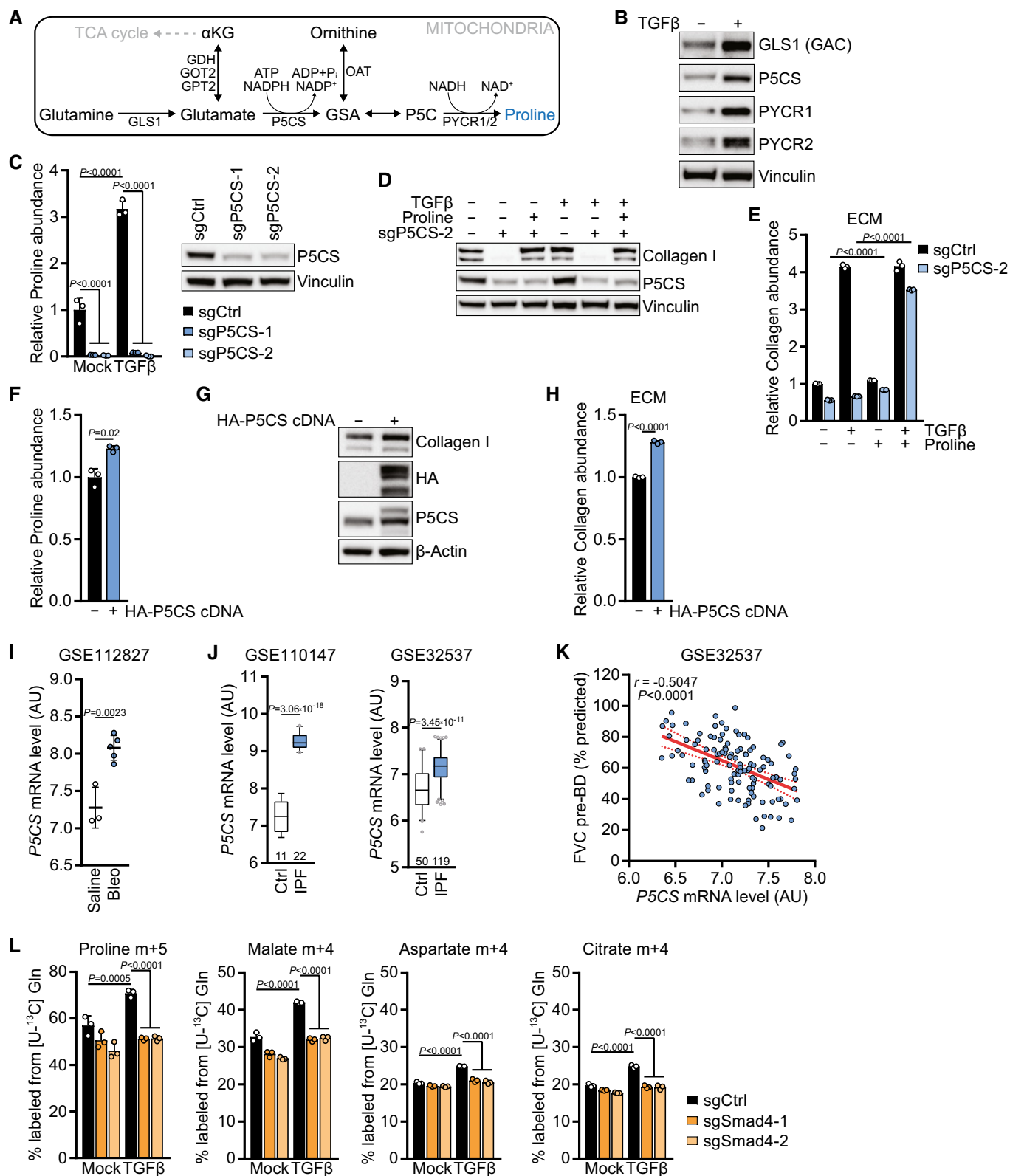


Figure 3.

Figure 3. P5CS is required for proline synthesis and upregulated in lung fibrosis patients.

- A Schematic of the mitochondrial proline biosynthetic pathway.
- B Western blot of NIH-3T3 cells treated with TGF β (2 ng/ml for all experiments) or mock for 48 h in the presence of 0.5% FBS.
- C Left: NIH-3T3 cells expressing sgCtrl, sgP5CS-1, or sgP5CS-2 were treated with TGF β or mock for 48 h, and proline abundance was measured by GC-MS. Values are relative to mock-treated sgCtrl-expressing cells. Right: Western blot of NIH-3T3 cells expressing sgCtrl, sgP5CS-1, or sgP5CS-2.
- D Western blot of NIH-3T3 cells expressing sgCtrl or sgP5CS-2 and treated with TGF β or mock for 48 h in the presence or absence of 0.15 mM proline.
- E Collagen abundance in ECM produced by NIH-3T3 cells expressing sgCtrl or sgP5CS-2 grown in the presence or absence of TGF β and 0.15 mM proline, measured by picrosirius red staining, and normalized to the packed cell volume of cells grown on a parallel plate under identical conditions. Values are relative to mock-treated sgCtrl-expressing cells.
- F Proline abundance in NIH-3T3 cells expressing empty vector or HA-P5CS cDNA, measured by GC-MS. Values are relative to mock-treated empty vector-expressing cells.
- G Western blot of NIH-3T3 cells expressing empty vector or HA-P5CS cDNA.
- H Collagen abundance in ECM produced by NIH-3T3 cells expressing empty vector or HA-P5CS cDNA, measured by picrosirius red staining, and normalized to the packed cell volume of cells grown on a parallel plate under identical conditions. Values are relative to mock-treated empty vector-expressing cells. $P < 0.0001$ (sgP5CS \pm proline in mock and TGF β -treated cells).
- I, J Analysis of the indicated gene expression datasets for mRNA levels of P5CS: (I) lung tissue from mice with pulmonary fibrosis induced by bleomycin (Bleo) treatment compared to saline treatment (GSE112827); (J) two datasets (GSE110147, GSE32537) from lungs of patients with idiopathic pulmonary fibrosis (IPF) compared to normal controls (Ctrl). AU, arbitrary units. The number of patients per group is indicated.
- K Pearson's correlation of P5CS mRNA level and forced vital capacity (FVC) before bronchodilator (pre-BD) as percentage of what was predicted for each patient, from clinical data of GSE32537.
- L Tracing of [^{13}C] L-glutamine ([^{13}C] Gln) into indicated metabolites. NIH-3T3 cells expressing sgCtrl, sgSmad4-1, or sgSmad4-2 were treated with TGF β or mock for 48 h, and the medium was replaced (including all treatments) with DMEM without L-glutamine and supplemented with [^{13}C] Gln for the last 8 h. Metabolites were measured by GC-MS.

Data information: P -values were calculated by two-sided unpaired t -test with Welch's correction (F, H), by two-way ANOVA with Holm-Sidak multiple comparison test (C, E, L), by moderated t -statistics and adjustment for multiple comparisons with the Benjamini and Hochberg false discovery rate method (I, J), or by Pearson's correlation (K). Bars in (C, E, F, H, L) represent the mean \pm SD; lines in (I) represent the mean \pm SD; data in (J) represent median with 50% confidence interval box and 95% confidence interval whiskers; and line in (K) represents linear regression with the SD shown as dotted lines. $n = 3$ (C, E, F, H, L); $n = 3$ (saline), $n = 5$ (bleomycin) (I); $n = 11$ (Ctrl, left), $n = 22$ (IPF, left), $n = 50$ (Ctrl, right), $n = 119$ (IPF, right) (J); $n = 117$ (K). A representative experiment is shown (B, C, D, G).

TGF β -induced stimulation of mitochondrial bioenergetics is required for increased proline biosynthesis

We next investigated the kinetics with which TGF β stimulates mitochondrial TCA cycle activity and oxidative phosphorylation. TGF β treatment increased mitochondrial respiration as soon as 6 h after TGF β addition (Fig 4A). While respiration reached a relative plateau after 24 h of treatment, the maximal respiratory capacity continued to increase beyond this time point (Fig 4B). Similarly, levels of glutamate and TCA cycle intermediates steadily increased from 6 to 48 h after TGF β treatment (Fig EV4E), indicating a progressive increase in mitochondrial TCA cycle flux after TGF β stimulation. These data indicate that TGF β continuously increases substrate availability to the ETC starting as soon as 6 h after the treatment, resulting in higher mitochondrial respiration and accumulation of mitochondrial redox potential.

Given that mitochondrial redox equivalents in the form of NADH and NADPH act as coenzymes for proline biosynthesis (Fig 3A), we hypothesized that an accumulation of mitochondrial redox potential drives proline biosynthesis in cells stimulated with TGF β . To test this idea, we genetically engineered NIH-3T3 cells to express a mitochondria-targeted version of the water-forming NADH oxidase from *Lactobacillus brevis* (*LbNOX*) or to express a mitochondria-targeted version of its NADPH-specific mutant triphosphopyridine nucleotide oxidase (*TPNOX*) (Titov *et al*, 2016; Cracan *et al*, 2017). As reported previously (Titov *et al*, 2016; Cracan *et al*, 2017), these cells displayed succinate accumulation and a reduced lactate/pyruvate ratio (Fig EV4F), a surrogate for the cytosolic NADH/NAD $^{+}$ ratio (Williamson *et al*, 1967). We observed that expression of either mitochondrial *LbNOX* or mitochondrial *TPNOX* reduced proline levels at baseline (Fig 4C). Notably, mitochondrial *LbNOX* or

mitochondrial *TPNOX* abrogated proline accumulation in response to TGF β stimulation (Fig 4C). These data suggest that an excess of mitochondrial redox potential beyond the electron assimilation capacity of the ETC can preferentially divert glutamine-derived glutamate into proline biosynthesis rather than into the TCA in response to TGF β (Fig 2I).

If mitochondrial redox potential is the sole regulator of proline biosynthesis, then inhibition of mitochondrial electron transport at complexes I and III might increase proline levels, as it results in an accumulation of NAD(P)H (Sullivan *et al*, 2015). As reported before (Mullen *et al*, 2014; Sullivan *et al*, 2015), treatment with rotenone, antimycin, or myxothiazol reduced aspartate levels and induced succinate and lactate accumulation (Fig EV4G), but decreased cellular proline levels (Fig 4D). Treatment with cobalt chloride (CoCl_2), which can contribute to mitochondrial damage by disrupting iron-sulfur clusters (Ranquet *et al*, 2007; Dai *et al*, 2008; Macomber & Imlay, 2009) that are present within aconitase and multiple ETC components, also reduced levels of proline, aconitate, and aspartate (Figs 4E and EV4H). Together, these results suggest that intact mitochondrial electron transport is critical to maintain proline levels.

Electron transport within the ETC generates a proton motive force across the mitochondrial inner membrane that drives ATP synthesis. To uncouple electron transport from the proton gradient, we applied carbonyl cyanide 4-(trifluoromethoxy)phenylhydrazone (FCCP) to cells treated with TGF β for 48 h. Addition of FCCP in the last 6 h of the treatment was sufficient to suppress proline accumulation (Fig 4F). As FCCP uncouples mitochondrial electron transport from ATP synthesis, these data suggest that TGF β -induced proline biosynthesis also depends on coupled electron transport to maintain mitochondrial ATP production. To test this directly, we applied the

ATP synthase inhibitor oligomycin to cells that had been stimulated with TGF β for 48 h, resulting in reduced levels of alpha-ketoglutarate but increased levels of glutamate and lactate (Fig EV4I). Notably, oligomycin treatment led to a progressive decrease in cellular proline levels both in untreated and TGF β -stimulated cells (Fig 4G). Thus, mitochondrial ATP synthesis is required for proline biosynthesis, likely for the reaction catalyzed by P5CS which consumes ATP (Fig 3A).

Proline biosynthesis is a vent for TGF β -induced mitochondrial redox stress

The above data indicate that TGF β promotes mitochondrial oxidative activity, resulting in an increased rate of ATP synthesis and the accumulation of NAD(P)H, and that both ATP and NAD(P)H accumulation are required to convert mitochondrial glutamine into proline. Consistent with this, we found that unlike other TGF β -induced mitochondrial metabolites (Fig EV4E), proline did not increase until after mitochondrial respiration reached a plateau at 24 h after TGF β treatment (Figs 4A and 5A). In fact, at earlier time points we found that TGF β -induced stimulation of mitochondrial metabolism was associated with increased ROS generation (Fig 5A). An excess of mitochondrial redox potential in response to increased mitochondrial oxidative metabolism can result in the generation of ROS (Murphy, 2009; Schieber & Chandel, 2014). We observed that ROS levels were increased 6 h after TGF β stimulation but declined over time and went back to baseline after 48 h despite continued treatment with TGF β (Fig 5A, see also Fig 1M). ROS were also transiently elevated in human lung fibroblasts 6 h after addition of TGF β to the culture medium (Fig EV5A). The timing of ROS increase correlated with the early increase in TCA cycle intermediates and mitochondrial respiration in response to TGF β stimulation (Figs 4A and EV4E), suggesting that TGF β -induced mitochondrial oxidative activity underlies the elevated ROS.

HIF-1 α is stabilized by mitochondrial ROS which are generated by excess substrate availability to the ETC (Chandel *et al*, 2000; Brunelle *et al*, 2005; Guzy *et al*, 2005; Bell *et al*, 2007; Lum *et al*, 2007). In agreement with higher mitochondrial substrate availability, TGF β also induced stabilization of HIF-1 α with similar kinetics as it induced ROS (Fig 5B). In line with Smad4 regulating glutaminolysis (Figs 3L and EV4D), ROS accumulation and HIF-1 α stabilization after 6 h TGF β treatment were dependent on Smad4 (Fig 5C and D), suggesting that the Smad4-dependent transcriptional program activated by TGF β induces glutaminolysis, ROS accumulation, and HIF-1 α stabilization. TGF β -induced HIF-1 α stabilization depended on mitochondrial ROS, as it was prevented by mitoquinol (MitoQ), a mitochondria-targeted antioxidant (Fig EV5B). To confirm whether TGF β -induced ROS were mitochondrial, we used either a mitochondria-targeted or a cytosol-targeted roGFP2 construct coupled to glutaredoxin (Grx1), allowing us to sensitively measure mitochondrial and cytosolic glutathione oxidation (Gutscher *et al*, 2008). Indeed, TGF β induced glutathione oxidation only in mitochondria, not in the cytosol after 6 h of treatment (Fig 5E). Taken together, these data suggest that TGF β activates glutaminolysis via Smad4, supporting TCA cycle anaplerosis, which increases substrate availability to the mitochondrial ETC, resulting in increased mitochondrial respiration and the generation of mitochondrial ROS that stabilize HIF-1 α . To test whether the

TGF β -induced transient stabilization of HIF-1 α plays a role in proline biosynthesis, we expressed sgRNAs targeting *HIF-1 α* , which prevented HIF-1 α stabilization after 6 h of TGF β stimulation (Fig EV5C). While cells expressing sg*HIF-1 α* displayed an increase in citrate and a decrease in lactate, proline levels were unchanged (Fig EV5D), indicating that HIF-1 α is not directly involved in proline upregulation in response to TGF β stimulation.

We next investigated how the decline of ROS levels observed after TGF β stimulation is regulated, despite ongoing mitochondrial oxidation and substrate accumulation (Fig 4A and B). We first tested whether TGF β promoted diversion of the first glycolytic intermediate glucose 6-phosphate (G6P) into the pentose phosphate pathway (PPP), which is a major producer of NADPH and is thus critical for antioxidant defense (Mullarky & Cantley, 2015). To analyze flux through the PPP, we traced the fate of glucose labeled at carbons one and two ([1,2-¹³C] Glc) and calculated the ratio of m+1 lactate (derived from PPP) to m+2 lactate (derived from glycolysis) (Lee *et al*, 1998). In line with elevated glucose uptake (Fig 1G), TGF β -treated cells displayed increased m+2 labeling of G6P which was diluted out in lactate (Fig EV5E and F). However, PPP activity was low and was not enhanced in response to TGF β treatment (Fig EV5G). These data suggest that TGF β does not stimulate flux through the PPP relative to glycolysis.

Under hypoxia, HIF-1 α -mediated metabolic reprogramming allows cells to divert glycolytic carbons away from mitochondrial oxidation to minimize ROS generation in the absence of a terminal electron acceptor (Lum *et al*, 2007). Similarly, proline biosynthesis could divert glutamine carbons away from mitochondrial oxidation and, in addition, uses up mitochondrial electrons that would otherwise be donated to the ETC (Fig 3A). This raised the intriguing possibility that TGF β -stimulated cells were using proline as a “vent” to prevent ROS generation due to the buildup of NADH in excess of the ability of oxidative phosphorylation to assimilate the extra electrons. To test whether activation of proline biosynthesis is important to resolve mitochondrial redox stress induced by TGF β , ROS levels were assessed in cells unable to engage in proline biosynthesis due to deletion of P5CS (Fig 3C), and grown in medium supplemented with proline to avoid effects of proline loss on protein translation and growth (Loayza-Puch *et al*, 2016; Sahu *et al*, 2016). While cells expressing sgCtrl did not display ROS after 48 h of TGF β stimulation, as described above (Figs 1M and 5A), cells expressing sg*P5CS* were unable to resolve TGF β -induced ROS (Fig 5F), indicating that the decline in ROS after 48 h of TGF β treatment depends on utilization of the proline biosynthetic pathway, not on proline itself. Taken together, these data indicate that proline biosynthesis functions in TGF β -induced mitochondrial oxidative metabolism to reduce ROS stress.

Mitochondrial citrate export limits proline biosynthesis and collagen production

If proline acts as a vent for redox stress imposed by increased TCA cycle activity, then we predicted that cells unable to engage in proline biosynthesis would utilize other vents to prevent excessive mitochondrial carbon oxidation and ROS accumulation in response to TGF β treatment. Consistent with this idea, we observed that *P5CS*-deleted cells displayed elevated levels of aspartate, citrate, and lactate when cultured in TGF β -containing medium (Fig EV5H), the

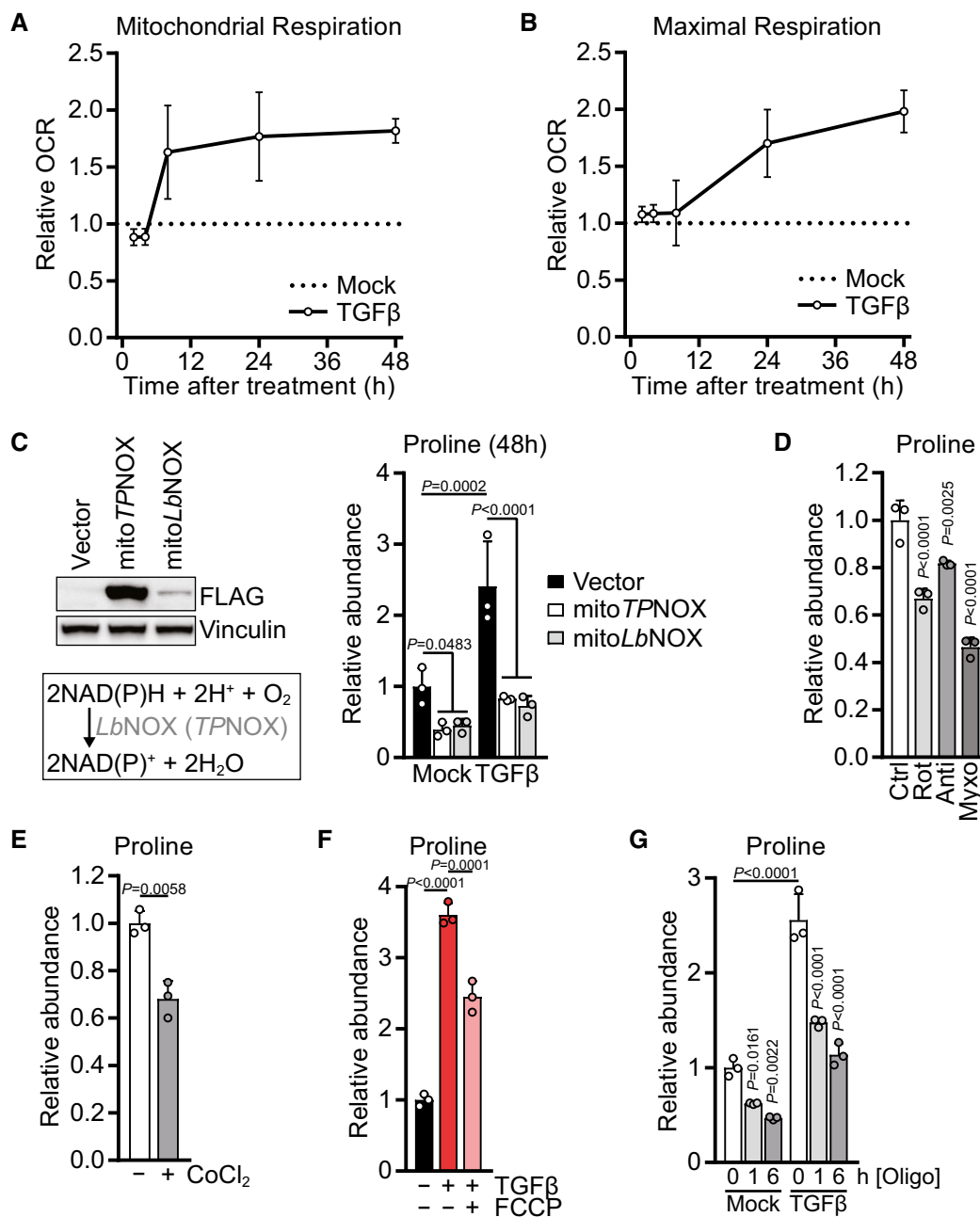


Figure 4. TGFβ-induced stimulation of mitochondrial bioenergetics is required for increased proline biosynthesis.

A, B Mitochondrial basal respiration (A) and FCCP-induced maximal respiration (B) of NIH-3T3 cells treated with TGFβ (2 ng/ml for all experiments) or mock for 2, 4, 8, 24 or 48 h, based on Seahorse OCR measurements. The relative values were calculated by normalizing the respective values of TGFβ-treated cells to those of mock-treated cells for each time point.

C Left: Western blot of NIH-3T3 cells expressing empty vector, mitoTPNOX, or mitoLbNOX. MitoTPNOX or mitoLbNOX expression is detected by probing for their FLAG-tag. Right: NIH-3T3 cells expressing empty vector, mitoTPNOX, or mitoLbNOX were treated with TGFβ or mock for 48 h, and proline abundance was measured by GC-MS. Values are normalized to mock-treated empty vector-expressing cells.

D NIH-3T3 cells were treated with rotenone, antimycin, myxothiazol, or vehicle control for 1 h, and proline abundance was measured by GC-MS. Values are normalized to control-treated cells.

E NIH-3T3 cells were treated with cobalt chloride (CoCl₂) or vehicle control for 6 h, and proline abundance was measured by GC-MS. Values are normalized to control-treated cells.

F NIH-3T3 cells were treated with TGFβ or mock for 48 h, and FCCP or vehicle control was added for the last 6 h of the treatment. Proline abundance was measured by GC-MS. Values are normalized to mock- and control-treated cells.

G NIH-3T3 cells were treated with TGFβ or mock for 48 h, and oligomycin or vehicle control was added for the last 1 or 6 h of the treatment. Proline abundance was measured by GC-MS. Values are normalized to mock- and control-treated cells.

Data information: P-values were calculated by two-way ANOVA with Holm–Sidak multiple comparison test (C, G), by one-way ANOVA with Holm–Sidak multiple comparison test (D, F), or by two-sided unpaired t-test with Welch’s correction (E). Bars in (C–G) represent the mean + SD; data in (A, B) represent the mean ± SD. n = 5–6 (A, B); n = 3 (C–G).

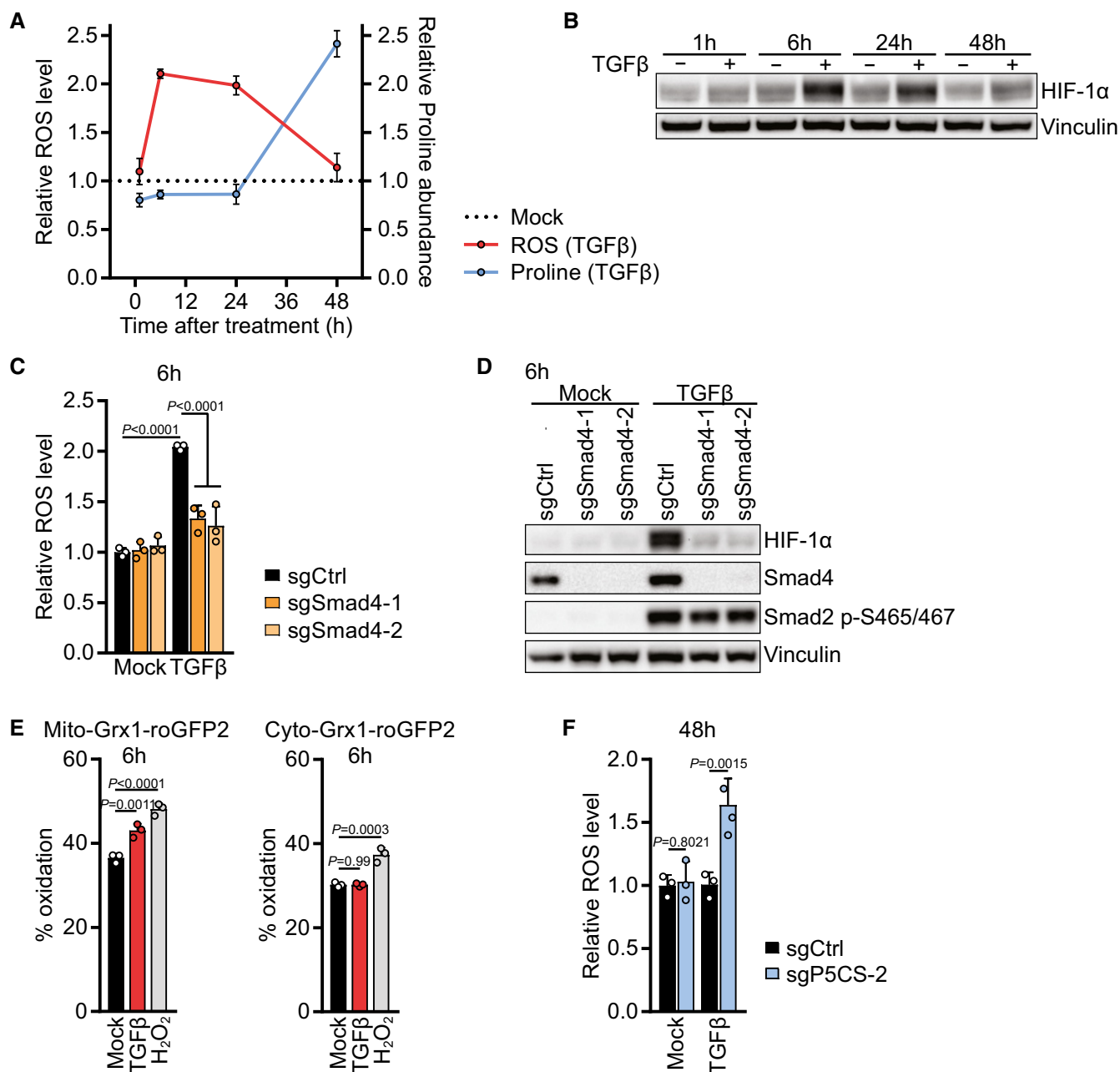


Figure 5. Proline biosynthesis is a vent for TGFβ-induced mitochondrial redox stress.

A NIH-3T3 cells were treated with TGFβ or mock for 1, 6, 24 or 48 h. ROS levels were measured by flow cytometry for CM-H₂DCFDA after incubation with CM-H₂DCFDA for the last 30 min of the treatment (Red line). Proline abundance was measured by GC-MS (Blue line). The relative levels were calculated by normalizing the respective values of TGFβ-treated cells to those of mock-treated cells for each time point.

B Western blot of NIH-3T3 cells treated with TGFβ or mock for 1, 6, 24 or 48 h.

C NIH-3T3 cells expressing sgCtrl, sgSmad4-1, or sgSmad4-2 were treated with TGFβ or mock for 6 h, and ROS levels were measured by flow cytometry for CM-H₂DCFDA after incubation with CM-H₂DCFDA for the last 30 min of the treatment. Values are normalized to mock-treated sgCtrl-expressing cells.

D Western blot of NIH-3T3 cells expressing sgCtrl, sgSmad4-1, or sgSmad4-2 and treated with TGFβ or mock for 6 h in the presence of 0.5% FBS.

E NIH-3T3 cells expressing mito-Grx1-roGFP2 or cyto-Grx1-roGFP2 were treated with TGFβ or mock for 6 h or with 100 μM H₂O₂ as a control. Emission was measured with a 520/10-nm filter after excitation with 405 nm and 488 nm lasers using flow cytometry. Oxidized roGFP2 gains excitability at 405 nm and loses excitability at 488 nm. Oxidation status is expressed as percentage of maximal oxidation which was determined by treating cells with 5 mM H₂O₂ for 5 min before harvest.

F NIH-3T3 cells expressing sgCtrl or sgP5CS-2 were treated with TGFβ or mock for 48 h in the presence of 0.15 mM proline. ROS levels were measured by flow cytometry for CM-H₂DCFDA after incubation with CM-H₂DCFDA for the last 30 min of the treatment.

Data information: *P*-values were calculated by two-way ANOVA with Holm-Sidak multiple comparison test (C, F) or by one-way ANOVA with Holm-Sidak multiple comparison test (E). Bars represent the mean + SD (C, E, F); data in (A) represent the mean ± SD. A representative experiment is shown (B, D).

alternative vents used by proliferating cells. In turn, we predicted that inhibition of mitochondrial citrate export in wild-type cells should result in elevated ROS levels and increased utilization of the proline biosynthetic pathway. Using 4-chloro-3-[(3-nitrophenyl)amino]sulfonyl-benzoic acid (CTPi), a competitive inhibitor of the mitochondrial citrate transport protein (CTP) (Aluvila *et al*, 2010), we found that cellular ROS levels increased in a dose-dependent fashion after 6 h of treatment to a similar extent as upon TGF β stimulation (Fig 6A). Similarly, inhibition of lactate dehydrogenase A (LDHAi) or activation of pyruvate kinase M2 (PKM2a) increased cellular ROS levels, although not to the same extent as did CTP inhibition (Fig EV5I).

To confirm the above results with a genetic approach, we deleted *Slc25a1* encoding CTP in NIH-3T3 cells (Fig 6B). Like the CTP inhibitor, *Slc25a1*-deleted cells displayed increased ROS levels which were further augmented upon 6-h TGF β treatment (Fig 6B). We hypothesized that blocking citrate export from mitochondria would increase mitochondria carbon load and, thus, TCA cycle activity, forcing cells to utilize other pathways to limit excessive mitochondrial oxidation. *Slc25a1* deletion resulted in a reduction in the cellular citrate pool (Fig EV5J) and a higher level of mitochondrial respiration and substrate availability, in particular in response to TGF β treatment (Fig EV5K). This indicated that citrate was oxidized in the TCA cycle, and consistent with that, levels of its downstream metabolites alpha-ketoglutarate and glutamate

were increased when *Slc25a1* was deleted, both in mock- and TGF β -treated cells (Fig EV5L). However, this increase was not observed in later TCA cycle intermediates such as malate and oxaloacetate-derived aspartate (Fig EV5L), possibly because CTP acts as a citrate–malate shuttle (Robinson *et al*, 1971), and thus, *Slc25a1* deletion might prevent import of malate into mitochondria. Notably, *Slc25a1* deletion caused an increase in the abundance of proline and synergized with TGF β treatment to elevate cellular proline levels more than ninefold (Fig 6C). These data suggest that when citrate export from mitochondria is blocked, cells adapt to reduce carbon oxidation in the TCA cycle by further increasing the preference of glutamine-derived carbons to enter the proline biosynthetic pathway.

Since proline biosynthesis is critical for collagen production (Fig 3D), we next asked whether fibroblasts handle proline accumulation induced by *Slc25a1* deletion by diverting it into collagen, which can then be secreted into the ECM. Consistent with the high abundance of proline when *Slc25a1* is deleted, these cells displayed elevated levels of collagen I but not fibronectin, an ECM protein which is not enriched in proline (Fig 6D). P5CS expression levels were similar in *Slc25a1*-deleted cells (Fig 6D), indicating that the increase in proline and collagen I cannot simply be explained by differential expression of the rate-limiting enzyme for proline biosynthesis. A higher abundance of collagen was also found in the ECM secreted by *Slc25a1*-deleted cells (Fig 6E). Conversely, ectopic

Figure 6. Mitochondrial citrate export limits proline biosynthesis and collagen production.

- A NIH-3T3 cells were treated with vehicle control or CTPi at increasing concentrations (0.1, 0.2, 0.5 mM) or TGF β (2 ng/ml for all experiments) for 6 h, and ROS levels were measured by flow cytometry for CM-H₂DCFDA after incubation with CM-H₂DCFDA for the last 30 min of the treatment. Values are relative to control-treated cells. *P*-values represent comparison of individual samples to the control.
- B Left: NIH-3T3 cells expressing sgCtrl, sg*Slc25a1-1*, or sg*Slc25a1-2* were treated with TGF β or mock for 6 h, and ROS levels were measured by flow cytometry for CM-H₂DCFDA after incubation with CM-H₂DCFDA for the last 30 min of the treatment. Values are relative to mock-treated sgCtrl-expressing cells. Right: Western blot of NIH-3T3 cells expressing sgCtrl, sg*Slc25a1-1*, or sg*Slc25a1-2*.
- C NIH-3T3 cells expressing sgCtrl, sg*Slc25a1-1*, or sg*Slc25a1-2* were treated with TGF β or mock for 48 h, and proline abundance was measured by GC-MS. Values are relative to mock-treated sgCtrl-expressing cells.
- D Western blot of NIH-3T3 cells expressing sgCtrl, sg*Slc25a1-1*, or sg*Slc25a1-2* and treated with TGF β or mock for 48 h.
- E Collagen abundance in ECM produced by NIH-3T3 cells expressing sgCtrl, sg*Slc25a1-1*, or sg*Slc25a1-2* grown in the presence or absence of TGF β , measured by picosirius red staining, and normalized to the packed cell volume of cells grown on a parallel plate under identical conditions. Values are relative to mock-treated sgCtrl-expressing cells.
- F NIH-3T3 cells expressing empty vector or *Slc25a1* cDNA were treated with TGF β or mock for 6 h, and ROS levels were measured by flow cytometry for CM-H₂DCFDA after incubation with CM-H₂DCFDA for the last 30 min of the treatment. Values are relative to mock-treated empty vector-expressing cells.
- G NIH-3T3 cells expressing empty vector or *Slc25a1* cDNA were treated with TGF β or mock for 48 h, and proline abundance was measured by GC-MS. Values are relative to mock-treated empty vector-expressing cells.
- H Western blot of NIH-3T3 cells expressing empty vector or *Slc25a1* cDNA and treated with TGF β or mock for 48 h.
- I Collagen abundance in ECM produced by NIH-3T3 cells expressing empty vector or *Slc25a1* cDNA grown in the presence or absence of TGF β , measured by picosirius red staining, and normalized to the packed cell volume of cells grown on a parallel plate under identical conditions. Values are relative to mock-treated empty vector-expressing cells.
- J, K Analysis of the indicated gene expression datasets for mRNA levels of *Slc25a1*, as described in Fig 3: (J) lung tissue from mice with pulmonary fibrosis induced by bleomycin (Bleo) treatment compared to saline treatment (GSE112827); (K) two datasets (GSE110147, GSE32537) from lungs of patients with idiopathic pulmonary fibrosis (IPF) compared to normal controls (Ctrl). AU, arbitrary units. The number of patients per group is indicated.
- L Pearson's correlation of *SLC25A1* and *P5CS* mRNA levels in IPF patients from GSE32537.
- M IPF patients from GSE32537 were assigned into *P5CS*^{low}/*SLC25A1*^{high} and *P5CS*^{high}/*SLC25A1*^{low} groups based on the expression level of *P5CS* and *SLC25A1*. "High" represents patients with *P5CS* or *SLC25A1* expression values being above the 75% percentile of the respective gene expression; "low" represents patients with expression values being below the 25% percentile of gene expression. The forced vital capacity (FVC) before bronchodilator (pre-BD) as percentage of what was predicted for each patient was compared between the groups.

Data information: *P*-values were calculated by two-way ANOVA with Holm–Sidak multiple comparison test (B, C, E–G, I), by one-way ANOVA with Holm–Sidak multiple comparison test (A), by moderated *t*-statistics and adjustment for multiple comparisons with the Benjamini and Hochberg false discovery rate method (J, K), by Pearson's correlation (L), or by two-sided unpaired *t*-test with Welch's correction (M). Bars in (A–C, E–G, I) represent the mean \pm SD; lines in (J) represent the mean \pm SD; data in (K, M) represent the median with 50% confidence interval box and 95% confidence interval whiskers; and line in (L) represents linear regression with the SD shown as dotted lines. *n* = 3 (A–C, E–G, I); *n* = 3 (saline), *n* = 5 (Bleo) (J); *n* = 11 (Ctrl, left), *n* = 22 (IPF, left), *n* = 50 (Ctrl, right), *n* = 119 (IPF, right) (K); *n* = 169 (L); *n* = 9 (*P5CS*^{low}/*SLC25A1*^{high}), *n* = 8 (*P5CS*^{high}/*SLC25A1*^{low}) (M). A representative experiment is shown (B, D, H).

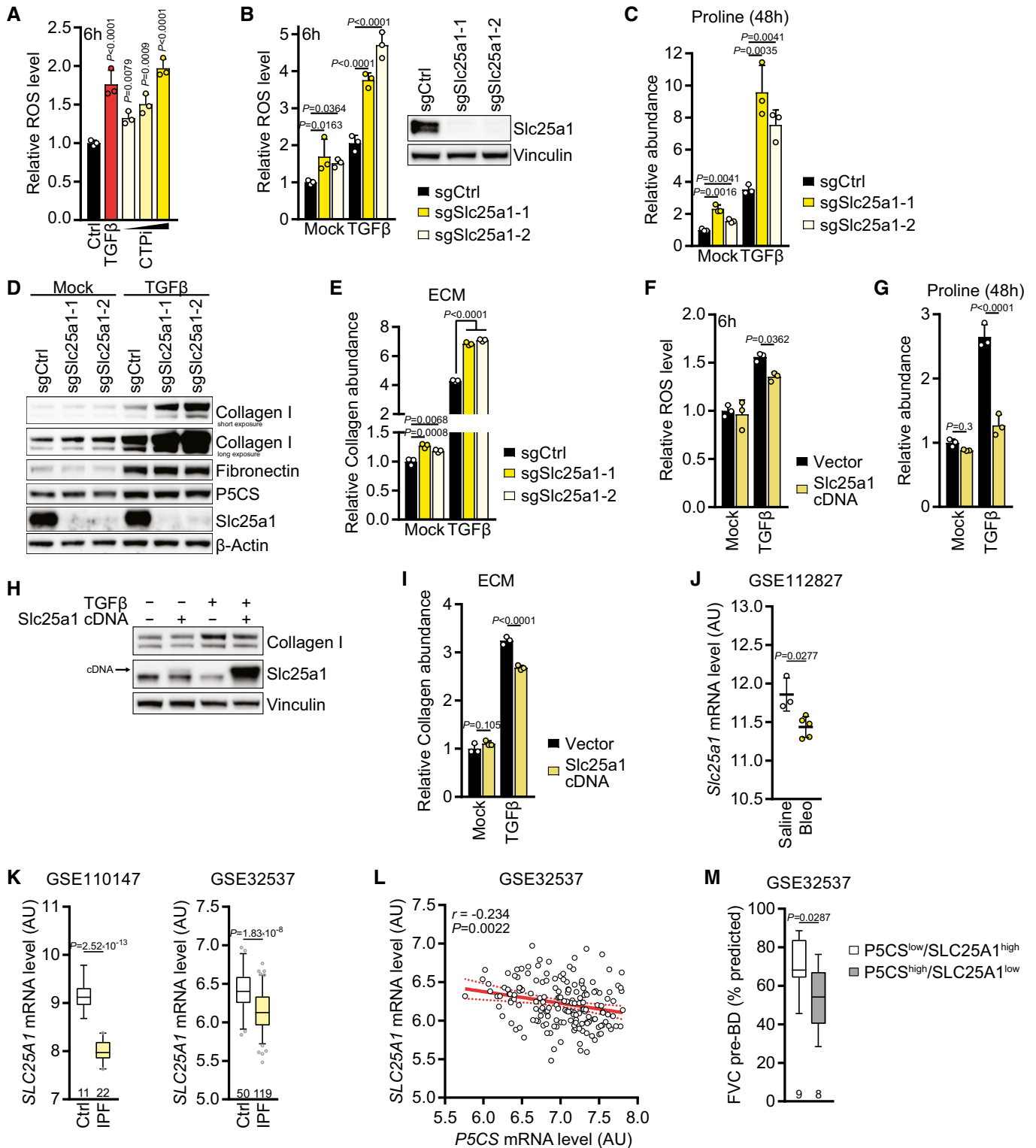


Figure 6.

expression of *Slc25a1* reduced cellular ROS levels, diminished proline accumulation, and led to a decline in collagen I levels in TGFβ-treated cells and their secreted ECM (Fig 6F–I). These results indicate that mitochondrial citrate export can limit proline biosynthesis and collagen production.

Based on these findings, we asked whether expression of *Slc25a1* was dysregulated in fibrotic disease. Consistent with *Slc25a1* deletion being sufficient to augment collagen levels, *Slc25a1* expression was downregulated in the bleomycin mouse model of pulmonary fibrosis (Fig 6J) as well as in IPF patients compared to normal

controls in two independent datasets (Fig 6K). In all datasets analyzed, *Slc25a1* expression inversely correlated with expression of *P5CS* (Figs 6L and EV5M and N). Since ectopic expression of *P5CS* and deletion of *Slc25a1* both increased collagen levels in the ECM (Figs 3H and 6E), we predicted that IPF patients concomitantly displaying elevated *P5CS* expression and downregulation of *SLC25A1* ($P5CS^{high}/SLC25A1^{low}$) would present impaired lung function due to excessive collagen deposition. Consistent with this idea, lung function was significantly compromised in such patients compared to patients with a $P5CS^{low}/SLC25A1^{high}$ expression profile (Fig 6M). Taken together, these data demonstrate that fibroblasts engage in proline biosynthesis and collagen production when mitochondrial oxidative metabolism is elevated, and that this process correlates with the impairment in lung function exhibited by patients with idiopathic pulmonary fibrosis.

Discussion

In this study, we provide evidence that in fibroblasts, TGF β is a potent stimulator of protein translation and nutrient uptake, reprogramming intermediate metabolism to promote both the production of the amino acids and the bioenergetic support for enhanced synthesis of matrix proteins. A major matrix component is collagens, triple-helical proteins whose individual building blocks are enriched in proline residues. This suggests that intracellular proline availability could limit the translation of proline-rich proteins such as collagen. To understand how TGF β selectively stimulated matrix production, we examined whether TGF β might exert its effects in part through stimulation of proline biosynthesis. First, we observed that TGF β induced proline biosynthesis in a Smad4-dependent manner. Second, we demonstrated that glutamine is preferentially used to support proline biosynthesis via *P5CS*, which requires an excess of mitochondrial NAD(P)H beyond which can be utilized for ATP synthesis. The subsequent incorporation of glutamine-derived proline into collagen then provided an adaptive sink for excess mitochondrial carbon when NAD(P)H and ATP are high. Therefore, increasing collagen production and secretion provides fibroblasts with an effective means to deal with the high mitochondrial redox potential generated by TGF β -mediated stimulation of glucose and glutamine metabolism.

We provide evidence that proline biosynthesis allows fibroblasts to prevent excessive ROS accumulation in response to a TGF β -induced mitochondrial redox potential. Proline accumulation in response to redox stress is a well-documented phenomenon in plants (Hayat *et al*, 2012). Stress-induced increase in proline levels in plants is a result of enhanced biosynthesis from glutamate (Hare & Cress, 1997), and knockout mutants of plant *P5CS* display a reduction of stress-induced proline biosynthesis, resulting in the accumulation of ROS (Székely *et al*, 2008). There is evidence that proline contributes to oxidative stress defense also in mammalian cells. The present data suggest that in the context of TGF β -stimulated fibroblasts, it is the consumption of mitochondrial NAD(P)H and ATP through proline biosynthesis from glutamine which contribute to ROS defense. In addition, other studies have demonstrated that proline itself may protect from oxidative damage by directly acting as ROS quencher (Kaul *et al*, 2008; Krishnan *et al*, 2008; Natarajan *et al*, 2012). Redox shuttling between proline and P5C via proline

dehydrogenase (PRODH) and PYCR has also been proposed to facilitate the transfer of NAD(P)H between mitochondria and the cytosol (Phang, 1985; Liu *et al*, 2015).

What regulates the preferential diversion of glutamate into proline biosynthesis, rather than into the TCA cycle? Our data suggest that the accumulation of both mitochondrial ATP and reducing equivalents contributes to the regulation of this process. This is consistent with earlier reports of reduced proline levels in cell lines with impaired mitochondrial function due to mutations in fumarase or mitochondrial DNA-encoded ETC components (Mullen *et al*, 2014; Chen *et al*, 2018). The oxidation of NADH in the ETC drives an electrochemical gradient that is used to synthesize ATP, and we found that uncoupling this gradient from ATP synthesis or direct inhibition of mitochondrial ATP synthase significantly reduces proline levels. ATP is, in addition to NADPH, required for the phosphorylation and reduction conversion of glutamate to P5C catalyzed by *P5CS*.

Consistent with the proposed role of TGF β in idiopathic pulmonary fibrosis, we find that expression of *P5CS* is upregulated in lungs of IPF patients, while *SLC25A1* is downregulated. We report that both *P5CS* and *Slc25a1* are regulators of proline biosynthesis and collagen production, and IPF patients with a $P5CS^{high}/SLC25A1^{low}$ expression profile display significantly impaired lung function. The present results also suggest that inhibition of mitochondrial electron transport might limit proline biosynthesis and collagen production in such patients. Notably, metformin, which targets complex I (Cameron *et al*, 2018), was shown to attenuate hepatic and pulmonary fibrosis in rodents (Gamad *et al*, 2018; Rangarajan *et al*, 2018), raising the possibility that the therapeutic effects could—at least in part—be due to inhibition of proline biosynthesis.

In conclusion, TGF β -induced proline biosynthesis is another example of how cells can handle an excess of intracellular metabolites when these are not used to support cell proliferation. Fibroblasts deal with the accumulating proline induced by TGF β by incorporating it into collagen, which is secreted into the ECM. This TGF β -induced conversion of available glucose and amino acids into enhanced extracellular matrix production would promote the regeneration of a damaged tissue during wound healing but, if stimulated in non-physiological ways, could lead to an excessive fibrotic reaction.

Materials and Methods

Cell culture

NIH-3T3 cells and IMR90 cells were obtained from ATCC and were cultured at 37°C in 5% CO₂ and 20% O₂. Cells were maintained in DMEM (25 mM D-glucose, 2 mM L-glutamine) supplemented with 10% FBS (Gemini), 100 units/ml penicillin, and 100 µg/ml streptomycin. The following supplements were added to the culture medium for maintenance of cells expressing the indicated guide RNAs: 0.15 mM L-proline (sg*P5CS*-expressing cells) and 1 mM sodium acetate (sg*Slc25a1*-expressing cells). All experiments with sg*P5CS*-expressing cells and all metabolite profiling experiments were done in DMEM supplemented with 10% dialyzed FBS (Gemini). For serum starvation experiments, the medium was changed to

DMEM supplemented with 0.5% FBS 5–6 h after plating of cells, and treatment was started 16–20 h later. All media were prepared by the media preparation facility at MSKCC. Cells were verified as mycoplasma-free by the MycoAlert Mycoplasma Detection Kit (Lonza).

Growth experiments

0.5×10^5 cells/well were plated in 12-well culture plates, and treatment was started 5–6 h later. Cell numbers at the start of treatment (d0) and 1–3 days later were counted in triplicates using the MultiSizer 3 Coulter Counter (Beckman) and normalized to the cell number at d0.

Chemicals

Antimycin (used at 1 μ M), CoCl_2 (100 μ M), CTPi (0.1–0.5 mM), DASA (PKM2a, 20 μ M), H_2O_2 (100 μ M), and myxothiazol (1 μ M) were purchased from Sigma; FCCP (2 μ M), mitoquinol (MitoQ, 1 μ M), oligomycin (1 μ M), and rotenone (0.5 μ M) were purchased from Cayman Chemical; GSK 2837808A (LDHAI, 10 μ M) was purchased from Tocris Bioscience; and TGF β -1 (2 ng/ml) was purchased from PeproTech.

Ectopic gene expression and CRISPR/Cas9-mediated gene deletion

P5CS cDNA, *mitoLbNOX*, and *mitoTPNOX* plasmids were obtained from Addgene and subcloned into a modified version of pTRE-Tight (Clontech) with addition of a C- or N-terminal HA-tag (*P5CS*) or FLAG-tag (*mitoLbNOX*, *mitoTPNOX*). *Slc25a1* cDNA plasmid was obtained from DNASU. Cyto- and *mito-Grx1-roGFP2* plasmids were obtained from Addgene. Guide RNAs targeting murine *HIF-1 α* , *P5CS*, *Pycr1*, *Pycr2*, *Smad4*, and *Slc25a1* (Table 1) were designed using GuideScan (<http://www.guidescan.com/>) and cloned into pLenti-CRISPRv2 (Addgene). Rosa26-targeting guides were used as a control. Polyclonal cell populations were used for the experiments. Lentiviral particles were produced in 293T cells by using psPAX2 and pCMV-VSV-G packaging plasmids (Addgene). Retroviral particles were produced in 293T cells by using pCG-gag-pol and pCMV-VSV-G packaging plasmids (Addgene). Viral supernatant was passed through a 0.45- μ m nylon filter and used to transduce NIH-3T3 cells in the presence of 8 μ g/ml polybrene (Sigma) overnight. Cells were subjected to puromycin (2 μ g/ml, Sigma), hygromycin (250 μ g/ml,

Millipore), or blasticidin (10 μ g/ml, InvivoGen) antibiotic selection the following day. Inducible expression of HA-*P5CS* cDNA, *mitoLbNOX*, and *mitoTPNOX* vectors was achieved with 100 ng/ml doxycycline (Sigma) and started when cells were plated for the experiment.

Western blot

Cells were lysed in 1 \times RIPA buffer (Millipore) supplemented with protease and phosphatase inhibitors (Thermo Fisher) on ice. Lysates were cleared by centrifugation for 10 min at 18,000 g and 4°C, and protein concentration was determined by BCA Protein Assay (Thermo Scientific). Equal amounts of protein were mixed with sample buffer and reducing agent (Thermo Scientific) and were separated on NuPAGE 4–12% Bis-Tris gels (Thermo Scientific). Proteins were transferred to nitrocellulose membranes, blocked for 1 h with 5% milk in TBS-T, and incubated in primary antibodies at 4°C overnight. Membranes were washed in TBS-T and incubated in HRP-coupled secondary antibodies at room temperature. Proteins were detected by chemiluminescence using ECL (Thermo Scientific) in a Bio-Rad ChemiDoc Imager. The following primary antibodies were used: vinculin (Sigma, V9131), β -actin (Sigma, A5441), α -tubulin (Sigma, T9026), collagen I (Abcam, ab21286), collagen IV (Proteintech, 55131-1-AP), fibronectin (Abcam, ab2413), puromycin (EMD Millipore, MABE343), GLS1 (Abcam, ab156876), *P5CS* (Sigma, HPA008333), *PYCR1* (Proteintech, 20962-1-AP), *PYCR2* (Proteintech, 17146-1-AP), HA-tag (Sigma, SAB4300603), FLAG-tag (Sigma, F1804), *Smad4* (Santa Cruz, sc-7966), *HIF-1 α* (Cayman Chemical, 10006421), *Smad2* phospho-S465/467 (Cell Signaling, 3108S), and *Slc25a1* (Proteintech, 15235-1-AP). The following secondary antibodies were used: anti-rabbit HRP (GE, NA934V) and anti-mouse HRP (Sigma, NA931).

Translation assays

For the assay involving Western blotting, cells were treated as indicated, and 90 μ M puromycin was added in the last 10 min of the experiment with or without 10 μ g/ml cycloheximide (CHX, Millipore) as control. Cells were lysed, and proteins were subjected to immunoblotting using an anti-puromycin antibody as described above. For the assay involving flow cytometry, cells were treated as indicated and incubated with 20 μ M O-propargyl-puromycin (OPP, Thermo Scientific) for the last 1 h of the experiment. Cells were harvested by trypsinization and fixed with methanol at -20°C , followed by permeabilization with 0.5% Triton X-100 in PBS. Cells were stained using the Click-iT Plus Alexa Fluor 647 Picolyl Azide Toolkit (Thermo Scientific) according to the manufacturer's instructions and analyzed by flow cytometry.

ECM extraction and collagen staining

Confluent NIH-3T3 or IMR90 cells were grown for 6 days on plates coated with 0.1% gelatin (Sigma) in the presence of 50 μ M ascorbate (Sigma) and treated as indicated, and the medium was replaced every other day. Plates were decellularized with 20 mM ammonium hydroxide/0.5% Triton X-100 for 5 min on a rotating platform. Three times the volume of PBS was added and ECM was equilibrated overnight at 4°C, followed by four additional PBS washes.

Table 1. Sequences of sgRNAs used in this study.

Gene	Guide 1 sequence	Guide 2 sequence
Ctrl (Rosa26)	GAAGATGGGCGGAGTCTTC	–
<i>HIF-1α</i>	TCGTTAGGCCAGTGAGAAA	CAAGATGTGAGCTCACATTG
<i>P5CS</i> (<i>Aldh18a1</i>)	CTTGCCGTGGGCACACTGA	GCCGCACGCTCTGAGACAGA
<i>Pycr1</i>	ACCCCGTCTGTGTACGGGA	ACGGTCTCGGCCCTCCGGGT
<i>Pycr2</i>	GCTGACCACGGCTCACCCG	CGTGGGCAGGTCCATATCCG
<i>Smad4</i>	AGACAGGCATCGTTACTTGT	AACTCTGTACAAGACCCGG
<i>Slc25a1</i>	CTTCACGTATTCGGTCGGGA	AGTGGTAGTCGTGTGCCCTA

Sample buffer supplemented with 1 mM DTT was added, ECM was scraped off, and proteins were separated by SDS-PAGE followed by immunoblotting. To measure collagen abundance, extracted ECM was stained with the Picro Sirius Red Stain Kit (Abcam) according to the manufacturer's instructions. The stain was extracted with 0.1 M NaOH, and optical density was measured at 550 nm using a microplate reader. Values were normalized to the packed cell volume (number \times volume) of cells grown on a separate plate under the same experimental conditions.

Measurement of glucose and glutamine consumption and lactate secretion

Cells were plated in 6-well cell culture plates at a concentration aimed to reach $0.5\text{--}1 \times 10^6$ cells at the time of harvest and treated with TGF β (2 ng/ml) for 48 h. Media were exchanged for an assay period of 12 h (+/– TGF β) in the last 12 h of the treatment period, then collected, centrifuged, and analyzed using a 2950 Biochemistry Analyzer (YSI Life Sciences) to determine glucose, glutamine, and lactate concentration. Absolute rates of consumption/secretion of these metabolites were calculated by subtracting the concentration in medium incubated for the same amount of time without cells and then normalizing to the cell number at the time of harvest, media volume, and hours of incubation. For time course experiments, treatments were started in a staggered fashion. For the 48- and 24-h treatments, TGF β was added before the 12-h assay period; for the 12-h treatment, TGF β was added when starting the assay period; for the 6- and 3-h treatments, TGF β was added during the assay period, such that the media for all conditions were harvested at the same time.

Measurement of oxygen consumption rate, extracellular acidification rate, ATP production rate, and glycolytic rate

Oxygen consumption rate (OCR), extracellular acidification rate (ECAR), ATP production rate (J_{ATP}), and glycolytic rate (glycoPER) were measured using a XFe96 Extracellular Flux Analyzer (Agilent). Cells were plated into Seahorse microplates (Agilent) at a density of 1.5×10^3 cells/well (10% FBS) or 5×10^3 cells/well (0.5% FBS), allowed to adhere overnight, and treated with TGF β (2 ng/ml) for 48 h. In the time course experiment, TGF β was added 2, 4, 8, 24 or 48 h before the assay. Treatment media were then removed and replaced with Seahorse media (DMEM containing 10 mM glucose, 2 mM glutamine, and 1 mM sodium pyruvate). OCR analysis was performed at basal level and after subsequent injections of oligomycin (1 μ M), FCCP (2 μ M), and rotenone/antimycin mix (0.5 μ M) according to the manufacturer's instructions. ECAR was analyzed at basal level without any injection. Mitochondrial respiration was defined as the last measurement before oligomycin injection subtracted by the minimum rate after rotenone/antimycin injection (non-mitochondrial respiration rate). Maximal respiration was calculated by subtracting the non-mitochondrial respiration rate from the maximum rate measurement after FCCP injection. Glycolytic (J_{ATPgly}) and oxidative (J_{ATPOX}) ATP production rates were calculated from Seahorse data according to Mookerjee *et al* (2017) using the bioenergetic spreadsheet downloaded from <https://russelljoneslab.vai.org/tools/>. For glycolytic rate analysis, treatment media were removed, cells were washed, and media were replaced with Seahorse media buffered

with 5 mM HEPES. The media were replaced with fresh assay media immediately before the assay. Glycolytic rate analysis was performed at basal level and after subsequent injections of rotenone/antimycin mix (0.5 μ M) and 2-DG (5 mM) according to the manufacturer's instructions, and glycoPER was calculated from the resulting OCR and ECAR data using WAVE software (Agilent) under default settings.

ROS measurement

Intracellular ROS levels were measured by the CM-H₂DCFDA general oxidative stress indicator (Thermo Scientific). Cells were incubated with 1 μ M CM-H₂DCFDA at 37°C for 30 min, harvested, and analyzed by flow cytometry. The mean fluorescence intensity of DAPI-negative cells was measured in the FITC channel.

Measurement of cytosolic and mitochondrial glutathione oxidation

Cells expressing cyto- or mito-Grx1-roGFP2 were treated with TGF β (2 ng/ml) for 6 h. Cells were washed and incubated with 20 mM N-ethylmaleimide (NEM, Sigma) for 5 min to prevent further probe oxidation. Cells were harvested, fixed with 4% formaldehyde, and analyzed by flow cytometry using a 520/10-nm filter. The ratio of emission after excitation at 405 and 488 nm was calculated as a measure of glutathione oxidation. The maximal oxidized and reduced form of the probe was determined for each experiment by incubating cells in extra wells with 5 mM H₂O₂ (Sigma) or 10 mM DTT (Thermo Scientific) for 5 min before adding NEM.

Stable isotope labeling and metabolite extraction

Cells were plated in 6-well cell culture plates at a concentration aimed to reach $0.5\text{--}1 \times 10^6$ cells at the time of harvest. For quantification of relative metabolite abundance, cells were treated with TGF β (2 ng/ml) for 48 h in DMEM supplemented with 10% dialyzed FBS (Gemini). For [U-¹³C] glutamine tracing experiments, cells were treated with TGF β for 48 h in DMEM supplemented with 10% FBS. In the last 2, 8 or 24 h, medium was replaced with DMEM without L-glutamine supplemented with 2 mM [U-¹³C] L-glutamine (Cambridge Isotope Laboratories) and 10% dialyzed FBS. For [U-¹³C] glucose and [1,2-¹³C] glucose tracing experiments, cells were treated with TGF β for 48 h in DMEM without L-serine and glycine supplemented with 0.5% dialyzed FBS. In the last 1, 8 or 24 h, medium was replaced with DMEM without D-glucose, L-serine, and glycine supplemented with 25 mM [U-¹³C] D-glucose (Cambridge Isotope Laboratories) or 25 mM [1,2-¹³C] D-glucose (Sigma) and 0.5% dialyzed FBS. For tracing of glutamine into serine and glycine, cells were treated with TGF β for 48 h in DMEM without L-serine and glycine supplemented with 0.5% dialyzed FBS. In the last 8 h, medium was replaced with DMEM without L-glutamine, L-serine, and glycine supplemented with 2 mM [U-¹³C] or [α -¹⁵N] L-glutamine (Cambridge Isotope Laboratories) and 0.5% dialyzed FBS. For relative quantification of metabolites by GC-MS, cells were washed briefly with PBS, which was then fully aspirated, and metabolism was quenched by immediately adding 1 ml of 80:20 methanol:water stored at –80°C containing 20 μ M deuterated 2-hydroxyglutarate (d5-2HG) as an internal standard. For relative

quantification of GSH and GSSG by LC-MS/MS, metabolism was quenched without the PBS washing step by adding 1 ml of 80:20 methanol:water stored at -80°C containing 1 $\mu\text{g}/\text{ml}$ deuterated SAM (d3-SAM, (RS)-S-adenosyl-L-methionine- d_3 (S-methyl- d_3) Tetra (*p*-toluenesulfonate); CDN Isotopes) and 2 $\mu\text{g}/\text{ml}$ deuterated SAH (d4-SAH, S-adenosylhomocysteine- d_4 ; Cayman Chemical). For stable isotope tracing experiments, metabolism was quenched without the PBS washing step by adding 1 ml of 80:20 methanol:water stored at -80°C . After overnight incubation at -80°C , the resulting mixtures were scraped on dry ice, transferred into a 1.5-ml centrifuge tube, and centrifuged at 20,000 *g* for 20 min at 4°C . The supernatants were collected in clean tubes and dried in a vacuum evaporator (Genevac EZ-2 Elite) for 2 h.

GC-MS measurement for TCA cycle metabolites and amino acids

Dried metabolite extracts were dissolved in 40 mg/ml methoxyamine hydrochloride (Sigma) in pyridine (Thermo Scientific) for 90 min at 30°C and derivatized with MSTFA with 1% TMCS (Thermo Scientific) for 30 min at 37°C . Samples were analyzed using an Agilent 7890A GC connected to an Agilent 5975C Mass Selective Detector with electron impact ionization. The GC was operated in splitless mode with constant helium gas flow at 1 ml/min. 1 μl of trimethylsilyl-derivatized metabolites was injected onto an HP-5MS column, and the GC oven temperature ramped from 60 to 290°C over 25 min. Peak ion chromatograms for metabolites of interest were recorded and extracted at their specific *m/z* with MassHunter Quantitative Analysis software v10.0 (Agilent Technologies). Ions used for quantification of metabolite levels are as follows: d5-2HG *m/z* 354; glycine *m/z* 174; serine *m/z* 204; aconitate *m/z* 375; citrate *m/z* 465; isocitrate *m/z* 245; alpha-ketoglutarate *m/z* 304; succinate *m/z* 247; fumarate *m/z* 245; malate *m/z* 335; aspartate *m/z* 232; proline *m/z* 216; glutamate *m/z* 246; glutamine *m/z* 245; lactate *m/z* 219; and pyruvate *m/z* 174. All peaks were manually inspected and verified relative to known spectra for each metabolite. For relative quantification, integrated peak areas were normalized to the internal standard d5-2HG and to the packed cell volume of each sample. Natural isotope abundance correction was performed with IsoCor software (Millard *et al*, 2012).

LC-MS measurement for TCA cycle metabolites and amino acids

Metabolite extracts were resuspended in 100 μl of 60:40 acetonitrile:water, vortexed well, and incubated on ice for 20 min. Samples were further clarified by centrifugation at 20,000 *g* for 20 min at 4°C , and the supernatant was used for LC-MS analysis. LC-MS measurement for TCA cycle metabolites and amino acids isotopic labeling was performed with a 6545 Q-TOF mass spectrometer with dual JetStream source (Agilent) operating in either positive or negative ion mode and coupled to hydrophilic interaction chromatography via electrospray ionization. For positive ionization mode, liquid chromatography separation was achieved on a ACQUITY UPLC BEH Amide column (150 mm \times 2.1 mm, 1.7 μm particle size, Waters) using a gradient of solvent A (10 mM ammonium acetate in 10:90 acetonitrile:water with 0.2% acetic acid, pH 4) and solvent B (10 mM ammonium acetate in 90:10 acetonitrile:water with 0.2% acetic acid, pH 4). The gradient was 0 min, 95% B; 9 min, 70% B; 13 min, 30% B; 14 min, 30% B; 14.5 min, 95% B; 15 min, 95% B;

and 20 min, 95% B. Other LC parameters were as follows: flow rate 400 $\mu\text{l}/\text{min}$, column temperature 40°C , and injection volume 5 μl . Other MS parameters were as follows: gas temp: 300°C ; gas flow: 10 l/min; nebulizer pressure: 35 psig; sheath gas temp: 350°C ; sheath gas flow: 12 l/min; VCap: 4,000 V; and fragmentor: 125 V. For negative ionization mode, liquid chromatography separation was achieved on a iHILIC-(P) Classic column (100 mm \times 2.1 mm, 5 μm particle size, HILICON) using a gradient of solvent A (10 mM ammonium bicarbonate in 10:90 acetonitrile:water with 5 μM medronic acid, pH 9.4) and solvent B (10 mM ammonium bicarbonate in 90:10 acetonitrile:water with 5 μM medronic acid, pH 9.4). The gradient was 0 min, 95% B; 15 min, 50% B; 18 min, 50% B; 19 min, 95% B; 19.10 min, 95% B; and 23 min, 95% B. Other LC parameters were as follows: flow rate 200 $\mu\text{l}/\text{min}$, column temperature 40°C , and injection volume 2 μl . Other MS parameters were as follows: gas temp: 300°C ; gas flow: 10 l/min; nebulizer pressure: 40 psig; sheath gas temp: 350°C ; sheath gas flow: 12 l/min; VCap: 3,000 V; and fragmentor: 125 V. Data were acquired from *m/z* 50 to 1,700 with active reference mass correction (*m/z*: 121.050873 and 922.009798 for acquisition in positive mode, and *m/z*: 119.0363 and 980.0163 for acquisition in negative mode) infused through a second nebulizer according to the manufacturer's instructions. Peak identification and integration were done based on exact mass and retention time match to commercial standards. Data analysis and natural isotope abundance correction were performed with MassHunter Profinder software v10.0 (Agilent Technologies). Flux from glutamine was calculated as the product of the first-order rate constant of the kinetic labeling curve and relative metabolite pool size (Yuan *et al*, 2008).

GSH and GSSG measurements with LC-MS/MS

The LC-MS/MS method for relative quantification of GSH and GSSG involved hydrophilic interaction chromatography (HILIC) coupled to the triple-quadrupole API 4000 mass spectrometer (Sciex). The LC separation was performed on a XBridge Amide column (50 mm \times 2.1 mm, 3.5 μm particle size, Waters, Milford, MA). Solvent A was 10:90 acetonitrile:water with 10 mM ammonium acetate and 0.2% acetic acid, and solvent B was 90:10 acetonitrile:water with 10 mM ammonium acetate and 0.2% acetic acid. The gradient was as follows: 0 min, 92% B; 6 min, 55% B; 9.5 min, 30% B; and 11 min, 92% B. Other LC parameters were as follows: flow rate 400 $\mu\text{l}/\text{min}$, column temperature 40°C , and injection volume 5 μl . The mass spectrometer was operated in positive MRM mode. Other MS parameters were as follows: curtain gas: 20 psi; nebulizer gas: 65 psi; heater gas: 60 psi; probe voltage: 4,000 V; probe temperature: 500°C ; and collision gas: 12 psi. Individual reactions that were monitored and collision energies (CE) were as follows: d3-SAM *m/z* 402.2 \rightarrow 301.1 (CE: 20 V)*, 250.2 (CE: 20 V); d4-SAH *m/z* 389.1 \rightarrow 253.9 (CE: 20 V)*, 140.4 (CE: 20 V); GSH *m/z* 308.1 \rightarrow 179.0 (CE: 20 V)*, 233.0 (CE: 20V); GSSG *m/z* 613.4 \rightarrow 484.0 (CE: 20 V)*, 355.0 (CE: 20 V), with * indicating the primary transition used to quantify each metabolite. Identities of metabolites were confirmed by presence of signal at both MRM transitions and by comparing to the retention times of pure standards. Data were analyzed using Analyst software v1.6.2 (SCIEX). Relative metabolite levels were quantified from raw peak areas corrected by d3-SAM or d4-SAH peak area factors and normalized to the packed cell volume.

Measurement of amino acid representation in proteins

Cellular lysates and ECM extracts were generated as described above. Acid hydrolysis was performed by incubating 200 µg cellular and ECM proteins in 1 ml 18% HCl containing 100 µM [U-¹³C, U-¹⁵N] labeled amino acid mix (Cambridge Isotope Laboratories) for 16 h at 100°C. Samples were cooled to room temperature and centrifuged at 20,000 g for 20 min. 500 µl supernatant was dried in a vacuum evaporator (Genevac EZ-2 Elite) for 2 h. Samples were prepared for GC-MS analysis as described above. Integrated peak areas of the unlabeled and fully labeled form of each amino acid were extracted, and their ratio was calculated. The sum of these ratios was calculated, and individual ratios were normalized to this sum to determine the percent representation of amino acids in proteins. Cysteine and tryptophan are acid-labile and were not detected. We also did not detect methionine in acid hydrolysates.

Proteomic analysis of stable isotope-labeled ECM

Confluent NIH-3T3 cells were cultured for 4 days on gelatin-coated plates in the presence of 50 µM ascorbate in DMEM without L-glutamine supplemented with 2 mM unlabeled [¹²C] L-glutamine or 2 mM [U-¹³C] L-glutamine and 10% dialyzed FBS, and medium was replaced after 2 days. ECM was extracted and subjected to SDS-PAGE as described above. Proteins were visualized by SimplyBlue SafeStain (Thermo Scientific) according to the manufacturer's instructions, and bands corresponding to collagen I were excised, enzymatically digested *in situ* with trypsin (Shevchenko *et al*, 2006), and desalted (Rappsilber *et al*, 2007). The purified peptides were diluted to 0.1% formic acid and analyzed by high-resolution LC-MS/MS in data-dependent mode. We used a Thermo Q Exactive Plus Orbitrap mass spectrometer coupled to a Waters nanoACQUITY system (with a 100-µm-inner diameter × 10-cm-long C18 column (1.7 µm BEH130; Waters)) configured with a 180 µm × 2 cm trap column. Trapping was performed at 15 µl/min buffer A for 1 min and peptide elution with a 50% linear acetonitrile gradient over 120 min. MS data were collected in data-dependent acquisition mode. Full scan MS1 spectra were acquired over 400–1,600 *m/z* at a resolution of 70,000 (*m/z* 400) with automatic gain control (AGC) at 1 × 10⁶ ions. The top 10 most intense precursor ions were selected for HCD fragmentation performed at normalized collision energy (NCE) 27 with target ion accumulation value of 5 × 10(4). MS/MS spectra were collected with a resolution of 17,500. Protein/peptide identifications from the LC-MS/MS data were performed using the Mascot search engine (Matrix Science, version 2.6.1.100; www.matrixscience.com) with the SwissProt mouse database (downloaded 20170705). The search parameters were as follows: (i) two missed cleavage tryptic sites were allowed; (ii) precursor ion mass tolerance = 10 ppm; (iii) fragment ion mass tolerance = 0.08 Da; and (iv) carbamidomethyl of cysteine was specified in Mascot as a fixed modification; and (v) deamidation of asparagine and glutamine, oxidation of methionine, acetyl of the N-terminus, and S,T,Y phosphor were specified in Mascot as variable modifications. Two peptides minimum and protein FDR threshold at 1%. Peptides corresponding to collagen I α-1 chain (CO1A1) were evaluated for their incorporation of the [¹³C] isotope from the samples cultured in the presence of [¹²C] or [U-¹³C] L-glutamine. Thermo Xcalibur version 2.2 and ICIS integration

algorithm were used to detect and integrate the area of each peak in the isotopomer.

Analysis of gene expression datasets and patient data

Processed gene expression datasets GSE112827, GSE110147, and GSE32537 were downloaded from Gene Expression Omnibus (GEO). Samples were assigned to groups and compared using GEOquery and limma packages from the Bioconductor project in R studio (www.r-project.org). *P*-values were adjusted for multiple comparison testing with the Benjamini and Hochberg false discovery rate method. Available clinical data for GSE32537 were correlated to individual gene expression profiles using Pearson's correlation analysis. Patients were grouped into low or high expressers according to the gene expression level being within the first or fourth quartile of the gene expression range.

Statistics

A Student *t*-test with Welch's correction was applied to compare one variable between two groups. One-way ANOVA was applied to compare one variable between three or more groups and corrected for multiple comparisons using the Holm–Sidak method. Two-way ANOVA was applied to compare two independent variables between two groups and corrected for multiple comparisons using the Holm–Sidak method. Pearson's correlation was applied to analyze correlation between data from two groups. *P*-values in gene expression datasets were calculated by moderate *t*-statistics and corrected for multiple comparisons with the Benjamini and Hochberg false discovery rate method with FDR < 1%. Statistical analysis was done using GraphPad Prism 7 software and R (v3.5.3). Graphs show the mean + SD with individual datapoints, unless indicated otherwise. Results are representative of at least two independent experiments.

Expanded View for this article is available online.

Acknowledgements

We thank the members of the Thompson laboratory for critical discussions during manuscript preparation. The authors thank B. King for cloning of *sgSmad4* constructs and T. Lindsten for critical reading of the manuscript. SS is supported by postdoctoral fellowships from the Human Frontier Science Program and the European Molecular Biology Organization. JZ is supported by the Leukemia and Lymphoma Society postdoctoral fellowship. JRC is supported by grants from the NIAID (R25 training grant AI140472-01A1) and the Donald B. and Catherine C. Marron Cancer Metabolism Center. This work is supported by grants from the NCI (CBT) and by the Cancer Center Support Grant (P30 CA008748) to MSKCC.

Author contributions

SS conceived the project, performed most experiments, analyzed the data, interpreted the results, and wrote the manuscript. MB and SV performed LC-MS measurements and analysis, and MB provided support for Seahorse experiments. WQ performed YSI measurements and assisted with GSH/GSSG measurements. JZ subcloned *P5CS*, *LbNOX*, and *TPNOX* constructs and provided support for some of the methods used in this study. RCH performed proteomic measurements and analysis. JRC supervised LC-MS and YSI experiments. CBT conceived the project, interpreted results, and wrote the manuscript.

Conflict of interest

CBT is a founder of Agios Pharmaceuticals and a member of its scientific advisory board. He is also a former member of the board of directors and stockholder of Merck and Charles River Laboratories. He holds patents related to cellular metabolism.

References

- Altman BJ, Stine ZE, Dang CV (2016) From Krebs to clinic: glutamine metabolism to cancer therapy. *Nat Rev Cancer* 16: 619–634
- Aluvila S, Sun J, Harrison DHT, Walters DE, Kaplan RS (2010) Inhibitors of the mitochondrial citrate transport protein: validation of the role of substrate binding residues and discovery of the first purely competitive inhibitor. *Mol Pharmacol* 77: 26–34
- Andrianifahanana M, Hernandez DM, Yin X, Kang JH, Jung MY, Wang Y, Yi ES, Roden AC, Limper AH, Leof EB (2016) Profibrotic up-regulation of glucose transporter 1 by TGF- β involves activation of MEK and mammalian target of rapamycin complex 2 pathways. *FASEB J* 30: 3733–3744
- Barrientos S, Stojadinovic O, Golinko MS, Brem H, Tomic-Canic M (2008) Growth factors and cytokines in wound healing. *Wound Repair Regen* 16: 585–601
- Bauer DE, Harris MH, Plas DR, Lum JJ, Hammerman PS, Rathmell JC, Riley JL, Thompson CB (2004) Cytokine stimulation of aerobic glycolysis in hematopoietic cells exceeds proliferative demand. *FASEB J* 18: 1303–1305
- Bauer DE, Hatzivassiliou G, Zhao F, Andreadis C, Thompson CB (2005) ATP citrate lyase is an important component of cell growth and transformation. *Oncogene* 24: 6314–6322
- Bell EL, Klimova TA, Eisenbart J, Moraes CT, Murphy MP, Budinger GRS, Chandel NS (2007) The Qo site of the mitochondrial complex III is required for the transduction of hypoxic signaling via reactive oxygen species production. *J Cell Biol* 177: 1029–1036
- Bernard K, Logsdon NJ, Benavides GA, Sanders Y, Zhang J, Darley-Usmar VM, Thannickal VJ (2018) Glutaminolysis is required for transforming growth factor- β 1-induced myofibroblast differentiation and activation. *J Biol Chem* 293: 1218–1228
- Birsoy K, Wang T, Chen WW, Freinkman E, Abu-Remaileh M, Sabatini DM (2015) An essential role of the mitochondrial electron transport chain in cell proliferation is to enable aspartate synthesis. *Cell* 162: 540–551
- Brunelle JK, Bell EL, Quesada NM, Vercauteren K, Tiranti V, Zeviani M, Scarpulla RC, Chandel NS (2005) Oxygen sensing requires mitochondrial ROS but not oxidative phosphorylation. *Cell Metab* 1: 409–414
- Cameron AR, Logie L, Patel K, Erhardt S, Bacon S, Middleton P, Harthill J, Forteach C, Coats JT, Kerr C *et al* (2018) Metformin selectively targets redox control of complex I energy transduction. *Redox Biol* 14: 187–197
- Cecchini MJ, Hosein K, Howlett CJ, Joseph M, Mura M (2018) Comprehensive gene expression profiling identifies distinct and overlapping transcriptional profiles in non-specific interstitial pneumonia and idiopathic pulmonary fibrosis. *Respir Res* 19: 1–12
- Chandel NS, McClintock DS, Feliciano CE, Wood TM, Melendez JA, Rodriguez AM, Schumacker PT (2000) Reactive oxygen species generated at mitochondrial Complex III stabilize hypoxia-inducible factor-1 α during hypoxia: a mechanism of O₂ sensing. *J Biol Chem* 275: 25130–25138
- Chen Q, Kirk K, Shurubor YI, Zhao D, Arreguin AJ, Shahi I, Valsecchi F, Primiano G, Calder EL, Carelli V *et al* (2018) Rewiring of glutamine metabolism is a bioenergetic adaptation of human cells with mitochondrial DNA mutations. *Cell Metab* 27: 1007–1025.e5
- Coultas DB, Zumwalt RE, Black WC, Sobonya RE (1994) The epidemiology of interstitial lung diseases. *Am J Respir Crit Care Med* 150: 967–972
- Cracan V, Titov DV, Shen H, Grabarek Z, Mootha VK (2017) A genetically encoded tool for manipulation of NAD⁺/NADPH in living cells. *Nat Chem Biol* 13: 1088–1095
- Dai RP, Yu FX, Goh SR, Chng HW, Tan YL, Fu JL, Zheng L, Luo Y (2008) Histone 2B (H2B) expression is confined to a proper NAD⁺/NADH redox status. *J Biol Chem* 283: 26894–26901
- Deberardinis RJ, Mancuso A, Daikhin E, Nissim I, Yudkoff M, Wehrli S, Thompson CB (2007) Beyond aerobic glycolysis: transformed cells can engage in glutamine metabolism that exceeds the requirement for protein and nucleotide synthesis. *Proc Natl Acad Sci USA* 104: 19345–19350
- Gamad N, Malik S, Suchal K, Vasisht S, Tomar A, Arava S, Arya DS, Bhatia J (2018) Metformin alleviates bleomycin-induced pulmonary fibrosis in rats: pharmacological effects and molecular mechanisms. *Biomed Pharmacother* 97: 1544–1553
- Gao P, Tchernyshyov I, Chang TC, Lee YS, Kita K, Ochi T, Zeller KI, De Marzo AM, Van Eyk JE, Mendell JT *et al* (2009) C-Myc suppression of miR-23a/b enhances mitochondrial glutaminase expression and glutamine metabolism. *Nature* 458: 762–765
- Gutscher M, Pauleau A-L, Marty L, Brach T, Wabnitz GH, Samstag Y, Meyer AJ, Dick TP (2008) Real-time imaging of the intracellular glutathione redox potential. *Nat Methods* 5: 553–559
- Guzy RD, Hoyos B, Robin E, Chen H, Liu L, Mansfield KD, Simon MC, Hammerling U, Schumacker PT (2005) Mitochondrial complex III is required for hypoxia-induced ROS production and cellular oxygen sensing. *Cell Metab* 1: 401–408
- Hamanaka RB, O’Leary EM, Witt LJ, Tian Y, Gökalp GA, Meliton AY, Dulin NO, Mutlu GM (2019) Glutamine metabolism is required for collagen protein synthesis in lung fibroblasts. *Am J Respir Cell Mol Biol* 0711: 1–37
- Hare PD, Cress WA (1997) Metabolic implications of stress-induced proline accumulation in plants. *Plant Growth Regul* 21: 79–102
- Hayat S, Hayat Q, Alyemeni MN, Wani AS, Pichtel J, Ahmad A (2012) Role of proline under changing environments: a review. *Plant Signal Behav* 7: 1456–1466
- Hosios AM, Hecht VC, Danaei LV, Johnson MO, Rathmell JC, Steinhauser ML, Manalis SR, Vander Heiden MG (2016) Amino acids rather than glucose account for the majority of cell mass in proliferating mammalian cells. *Dev Cell* 36: 540–549
- Ignotz RA, Massagué J (1986) Transforming growth factor-beta stimulates the expression of fibronectin and collagen and their incorporation into the extracellular matrix. *J Biol Chem* 261: 4337–4345
- de Ingeniis J, Ratnikov B, Richardson AD, Scott DA, Aza-Blanc P, De SK, Kazanov M, Pellicchia M, Ronai Z, Osterman AL *et al* (2012) Functional specialization in proline biosynthesis of melanoma. *PLoS ONE* 7: e45190
- Kaul S, Sharma SS, Mehta IK (2008) Free radical scavenging potential of L-proline: evidence from *in vitro* assays. *Amino Acids* 34: 315–320
- Krishnan N, Dickman MB, Becker DF (2008) Proline modulates the intracellular redox environment and protects mammalian cells against oxidative stress. *Free Radic Biol Med* 44: 671–681
- Lee WNP, Boros LG, Puigjaner J, Bassilian S, Lim S, Cascante M (1998) Mass isotopomer study of the nonoxidative pathways of the pentose cycle with [1,2-¹³C]glucose. *Am J Physiol Endocrinol Metab* 274: 843–851
- Lien EC, Lyssiotis CA, Juvekar A, Hu H, Asara JM, Cantley LC, Toker A (2016) Glutathione biosynthesis is a metabolic vulnerability in PI(3)K/Akt-driven breast cancer. *Nat Cell Biol* 18: 572–578

- Liu W, Hancock CN, Fischer JW, Harman M, Phang JM (2015) Proline biosynthesis augments tumor cell growth and aerobic glycolysis: involvement of pyridine nucleotides. *Sci Rep* 5: 1–13
- Loayza-Puch F, Rooijers K, Buil LCM, Zijlstra J, Oude Vrielink JF, Lopes R, Ugalde AP, Van Breugel P, Hofland I, Wesseling J et al (2016) Tumour-specific proline vulnerability uncovered by differential ribosome codon reading. *Nature* 530: 490–494
- Lum JJ, Bui T, Gruber M, Gordan JD, DeBerardinis RJ, Covello KL, Simon MC, Thompson CB (2007) The transcription factor HIF-1 α plays a critical role in the growth factor-dependent regulation of both aerobic and anaerobic glycolysis. *Genes Dev* 21: 1037–1049
- Macomber L, Imlay JA (2009) The iron-sulfur clusters of dehydratases are primary intracellular targets of copper toxicity. *Proc Natl Acad Sci USA* 106: 8344–8349
- Massagué J (2012) TGF β signalling in context. *Nat Rev Mol Cell Biol* 13: 616–630
- Millard P, Letisse F, Sokol S, Portais J-C (2012) IsoCor: correcting MS data in isotope labeling experiments. *Bioinformatics* 28: 1294–1296
- Mookerjee SA, Gerencser AA, Nicholls DG, Brand MD (2017) Quantifying intracellular rates of glycolytic and oxidative ATP production and consumption using extracellular flux measurements. *J Biol Chem* 292: 7189–7207
- Mullarky E, Cantley LC (2015) Diverting glycolysis to combat oxidative stress. In *Innovative Medicine*, Nakao K, Minato N, Uemoto S (eds), Tokyo: Springer
- Mullen AR, Hu Z, Shi X, Jiang L, Boroughs LK, Kovacs Z, Boriack R, Rakheja D, Sullivan LB, Linehan WM et al (2014) Oxidation of alpha-ketoglutarate is required for reductive carboxylation in cancer cells with mitochondrial defects. *Cell Rep* 7: 1679–1690
- Murphy MP (2009) How mitochondria produce reactive oxygen species. *Biochem J* 417: 1–13
- Natarajan SK, Zhu W, Liang X, Zhang L, Demers AJ, Zimmerman MC, Simpson MA, Becker DF (2012) Proline dehydrogenase is essential for proline protection against hydrogen peroxide-induced cell death. *Free Radic Biol Med* 53: 1181–1191
- Nigdelioglu R, Hamanaka RB, Meliton AY, O'Leary E, Witt LJ, Cho T, Sun K, Bonham C, Wu D, Woods PS et al (2016) Transforming growth factor (TGF)- β promotes *de novo* serine synthesis for collagen production. *J Biol Chem* 291: 27239–27251
- Phang JM (1985) The regulatory functions of proline and pyrroline-5-carboxylic acid. *Curr Top Cell Regul* 25: 91–132
- Rangarajan S, Bone NB, Zmijewska AA, Jiang S, Park DW, Bernard K, Locy ML, Ravi S, Deshane J, Mannon RB et al (2018) Metformin reverses established lung fibrosis in a bleomycin model. *Nat Med* 24: 1121–1131
- Ranquet C, Ollagnier-de-Choudens S, Loiseau L, Barras F, Fontecave M (2007) Cobalt stress in *Escherichia coli*: the effect on the iron-sulfur proteins. *J Biol Chem* 282: 30442–30451
- Rappsilber J, Mann M, Ishihama Y (2007) Protocol for micro-purification, enrichment, pre-fractionation and storage of peptides for proteomics using StageTips. *Nat Protoc* 2: 1896–1906
- Rathmell JC, Heiden MG, Harris MH, Frauwirth KA, Thompson CB (2000) In the absence of extrinsic signals, nutrient utilization by lymphocytes is insufficient to maintain either cell size or viability. *Mol Cell* 6: 683–692
- Robinson BH, Williams GR, Halperin ML, Leznoff CC (1971) Factors affecting the kinetics and equilibrium of exchange reactions of the citrate-transporting system of rat liver mitochondria. *J Biol Chem* 246: 5280–5286
- Sahu N, Dela Cruz D, Gao M, Sandoval W, Haverty PM, Liu J, Stephan JP, Haley B, Classon M, Hatzivassiliou G et al (2016) Proline starvation induces unresolved ER stress and hinders mTORC1-dependent tumorigenesis. *Cell Metab* 24: 753–761
- Schieber M, Chandel NS (2014) ROS function in redox signaling and oxidative stress. *Curr Biol* 24: R453–R462
- Selvarajah B, Azuelos I, Platé M, Guillotin D, Forty EJ, Contento G, Woodcock H V, Redding M, Taylor A, Brunori G et al (2019) mTORC1 amplifies the ATF4-dependent *de novo* serine-glycine pathway to supply glycine during TGF- β 1 –induced collagen biosynthesis. *Sci Signal* 12: eaav3048
- Shevchenko A, Tomas H, Havli J, Olsen JV, Mann M (2006) In-gel digestion for mass spectrometric characterization of proteins and proteomes. *Nat Protoc* 1: 2856–2860
- Siegel PM, Massagué J (2003) Cytostatic and apoptotic actions of TGF- β in homeostasis and cancer. *Nat Rev Cancer* 3: 807–820
- Sullivan LB, Gui DY, Hosios AM, Bush LN, Freinkman E, Vander Heiden MG (2015) Supporting aspartate biosynthesis is an essential function of respiration in proliferating cells. *Cell* 162: 552–563
- Székely G, Abrahám E, Csépló A, Rigó G, Zsigmond L, Csiszár J, Ayaydin F, Strizhov N, Jásik J, Schmelzer E et al (2008) Duplicated P5CS genes of Arabidopsis play distinct roles in stress regulation and developmental control of proline biosynthesis. *Plant J* 53: 11–28
- Thompson CB (2011) Rethinking the regulation of cellular metabolism. *Cold Spring Harb Symp Quant Biol* 76: 23–29
- Titov DV, Cracan V, Goodman RP, Peng J, Grabarek Z, Mootha VK (2016) Complementation of mitochondrial electron transport chain by manipulation of the NAD⁺/NADH ratio. *Science* 352: 231–235
- Vander Heiden MG, Cantley LC, Thompson CB (2009) Understanding the Warburg effect: the metabolic requirements of cell proliferation. *Science* 324: 1029–1033
- Wellen KE, Thompson CB (2010) Cellular metabolic stress: considering how cells respond to nutrient excess. *Mol Cell* 40: 323–332
- Williamson DH, Lund P, Krebs HA (1967) The redox state of free nicotinamide-adenine dinucleotide in the cytoplasm and mitochondria of rat liver. *Biochem J* 103: 514–527
- Wise DR, DeBerardinis RJ, Mancuso A, Sayed N, Zhang X-Y, Pfeiffer HK, Nissim I, Daikhin E, Yudkoff M, McMahon SB et al (2008) Myc regulates a transcriptional program that stimulates mitochondrial glutaminolysis and leads to glutamine addiction. *Proc Natl Acad Sci USA* 105: 18782–18787
- Yang IV, Coldren CD, Leach SM, Seibold MA, Murphy E, Lin J, Rosen R, Neidermyer AJ, McKean DF, Groshong SD et al (2013) Expression of cilium-associated genes defines novel molecular subtypes of idiopathic pulmonary fibrosis. *Thorax* 68: 1114–1121
- Yuan J, Bennett BD, Rabinowitz JD (2008) Kinetic flux profiling for quantitation of cellular metabolic fluxes. *Nat Protoc* 3: 1328–1340